Solid State Phenomena
ISSN: 1662-9779, Vol. 293, pp 1-34
doi:10.4028/www.scientific.net/SSP.293.1

Submitted: 2019-02-11
Revised: 2019-04-02
Accepted: 2019-04-02
Online: 2019-07-09

Optical and Electrical Investigation of Electrospun PAN/TiO_2, Bi_2O_3, SiO_2 Composite Thin Films

Wiktor Matysiak[1, a *]

[1]Institute of Engineering Materials and Biomaterials, Silesian University of Technology, Konarskiego 18A, 44-100 Gliwice, Poland

[a]wiktor.matysiak@polsl.pl

Keywords: electrospinning method, nanofibers, nanocomposites, nanoparticeles, optical properties, electrical properties

Abstract. The aim of study was to produce a nanocomposite polymer fibrous thin films, with the participation of the reinforcing phase in the form of TiO2/Bi2O3/SiO2 nanoparticles with a matrix of polyacrylonitrile (PAN), made by electrospinning of solution and investigation of optical and electrical properties of obtained nanomaterials. To determination of structore of used ceramic nanoparticles the X-ray diffraction analysis (XRD) was carrying out. The morphology of the obtained polymeric and composite fibrous mats and dispersion of nanoparticles in their volume was examined using scanning electron microscopy (SEM). All the physical properties of which were: the dielectric constant, and refractive index were tested and plotted against the concentration by weight of the used reinforcing phase which was as follows: 0%, 4%, 8%, 12% for each type of nanoparticles. The optical and electrical constants of obtained thin folms was performed on the basis of UV-Vis spectra of absorbance as a function of the wavelength. Using two methods: the method proposed by the author and the recorded absorbance spectra and spectroscopic ellipsometry determined the refractive index n, real n' and imaginary k part of the refractive index as a function of the wavelength, complex dielectric permeability ε, real and imaginary parts ε_r and ε_i of the dielectric permeability as a function of the wavelength of the polimeric and composite fibrous thin films.

Introduction

Until the present day, many papers have been published — the majority of which have been papers authored by a scientific team led by Reneker [1-13] — covering an analysis of the influences of the electrospinning process parameters on the morphology of the obtained nano-scale polymer fibres. There is, however, a lack of complex literature references, in which the influence of the type and concentration of nano-scale particles used as the reinforcement phase, on the morphology of polymer nano-scale fibres produced with electrospinning technology would be analysed. There is also a lack of information pertaining to the influence of other parameters of the electrospinning process on the morphology and qualities of the obtained nano-scale polymer fibres/particles. A literature overview with the use of Science Direct and Google Scholar databases indicated merely ten papers in the field of production and analysis of the influence of the used nano-scale TiO_2 or SiO_2 particles on the morphology of nano-scale composite fibres in a polyacrylonitrile (PAN) or polyvinylpyrrolidone (PVP) matrix.

In their work [14], Toni E. Newsome and Susan V. Olesik presented a method of producing nano-scale composite fibres in a polyvinylpyrrolidone matrix, reinforced with nano-scale silica particles, with diameters of 250 nm. The base of the spinning solution was a mixture of ethanol, methanol and propanol with a percentage share of, respectively, 90%:5%:5% (the paper's authors did not provide information whether the percentage share of the used alcohols was the volume or the mass). The PVP polymer was added to such a mixture of solvents, and thus three PVP/EtOH/MeOH/PrOH polymer solutions were obtained. Wherein with relative to the solvent mixture polymer mass concentration of respectively were 9%, 10% and 11%. The next stage was to prepare a second type of mixtures, consisting in the abovementioned ethanol, methanol and 1-propanol mixture with nano-scale silica particles with mass concentrations relative to the used alcohol mixture of, respectively, 20%, 25% and 30%. The final spinning solutions were obtained through mixing of each type of the first group

of mixtures, i.e. PVP/EtOH/MeOH/PrOH with the second type, i.e. SiO_2/EtOH/MeOH/PrOH, each time employing a mass ratio of 2:3. In order to obtain nano-scale composite fibres, Newsome and Olesik used the electrospinning method with the applied process parameters of, respectively: distance and potential difference between electrodes amounting to 10 cm and 10 kV, and the spinning solution feed rate amounting to 4 l/min. In order to analyse the influence of the mass concentration of a polymer in a spinning solution on the morphology of the obtained PVP/SiO2 nanofibres, the solutions of PVP/EtOH/MeOH/PrOH were mixed in a 2:3 ratio with 20% mixture of SiO2 NPs/EtOH/MeOH/PrOH. The morphological analysis of the obtained composite fibre mats was conducted with the use of SEM topography images of their surface. Research results indicated that irrespective of the employed polymer concentration in the spinning solution, the obtained nano-scale fibres featured an even dispersion of nano-scale particles across the whole volume of the nano-scale fibres. However, if in the process of electrospinning the solution containing the smallest amount of polymer was used, it contributed to resulting nano-scale fibres featuring numerous structural defects, in the form of the so-called 'spherical beads'. There were no such structural defects present in PVP/SiO2 nanofibers obtained with the use of the remaining two spinning solutions, prepared with the use of PVP/EtOH/MeOH/PrOH mixtures containing, respectively, 10% and 11% of polymer. Spherical bead defects, spaced along the entire length of single composite nanofibers, were probably generated due to a too low viscosity of the spinning solution used for their spinning. Additionally, the analysis of the diameters of single composite nanofibers of each sample, conducted on the basis of SM images of fibre mats, indicated a considerable increase in the diameters of the measured nano-scale fibres that was accompanied by an increase in the mass share of polyvinylpyrrolidone in the spinning solution. An increase of the polymer concentration in the spinning solution by merely 1% — from 10% to 11% — resulted in an increase of the mean diameter of nano-scale fibres from 380 nm to 430 nm. On the basis of the above analyses, the authors of the paper [14] selected a spinning solution containing 10% of PVP as the most optimal one, making it possible to obtain nanometric PVP composite fibres/nano-scale SiO_2 particles without structural defects, and used them for running an analysis of the influence of the mass concentration of nano-scale silica particles in the spinning solution on the morphology of the obtained nano-scale composite fibres. To this end, Newsome and Olesik mixed a 10% PVP/EtOH/MeOH/PrOH polymer solution in a 2:3 ratio with, successively, SiO_2/EtOH/MeOH/PrOH mixtures in which the concentration of nano-scale particles amounted to 20%, 25% and 30%. In this case, each group of the obtained thin fibre mats featured nano-scale fibres lacking structural defects in the form of beads. Similarly as in the case of an increase of the polymer mass concentration in the spinning solution, an increase of the mass share of the used nano-scale silica particles resulted in an increase of the diameters of the obtained nano-scale composite fibres, starting with 380 nm for 20% SiO_2 concentration, up to 540 nm for nano-scale fibres containing 30% of nano-scale particles of the reinforcement phase. Unequivocally, the conducted analyses prove an increase in the spinning solution viscosity due to an increase in the share of nano-scale ceramic particles in the spinning solution, which, in turn, leads to an increase in the diameters of the spun nano-scale polymer fibres.

In 2[illegible] C. Bahsari et al. presented in their paper [15] a method of obtaining nano-scale fibres in a polyacrylonitrile matrix, containing nano-scale titanium oxide particles, featuring a porous structure. The aim of their work was to devise a carrier for nano-scale TiO_2 particles, which due to their large specific surface area, stemming from their sizes in the nanometric scale, featured very good photocatalytic characteristics. Attempts of dispersing nano-scale particles in liquids did not yield the expected results due to the coagulation process of nano-scale particles, which aggregated and, in turn, decreased the active area of contact of reagents with the surface of nano-scale TiO_2 particles, acting as a catalyst. Subsequent efforts of finding a suitable carrier for nano-scale particles, with a concurrent retention of their active contact area, consisted in the creation of nano-scale PAN/TiO_2 fibres with the application of the electrospinning method using a polymer solution. Nano-scale composite fibres were spun with three types of solutions. The first type was 5% (mass) PAN solution in dimethylformamide (DMF), containing, respectively, 0%, 1%, 2% and 3% of nano-scale titanium oxide particles relative to the mass of the prepared solution. The second spinning solution,

except for nano-scale TiO_2 particles (0%, 1%, 2% and 3% of mass), polyacrylonitrile and dimethylformamide (DMF) with 5% mass polymer concentration relative to the entire mass of the mixture, also included 3% of mass of water (H_2O). The third solution featured the same components as the second one, but the concentration of water in the mixture was increased from 3% to 5%. These solutions were subjects of the electrospinning process, under constant process parameters, that is: distance between electrodes amounting to 10 cm and potential difference amounting to 20 kV. The spinning solution flow rate was set at 0.012 mL/min for the first type of solutions and 0.025 mL/min for the spinning solutions containing water. A surface topography analysis of the obtained nano-scale PAN polymer fibres and PAN/TiO_2 composite fibres conducted with the use of a scanning electron microscope indicated that nano-scale fibres obtained from the first type of spinning solution, i.e. the one not containing water, featured the smallest diameters. The obtained results indicated that PAN and PAN/TiO_2 fibres featured diameters of 170–220 nm, with diameters of single fibres increasing concurrently with an increase of the concentration of the used nano-scale particles from 0% to 3% of mass. The employment of solutions containing water favoured spinning of nano-scale fibres with mean diameters of 240–305 nm for the solution with 3% share of H_2O, and 340–430 nm for the solution with 5% share of water in the mixture. Also, in these cases, an increase in the diameters of the nano-scale fibres, accompanying the increasing mass concentration of the used nano-scale titanium oxide particles, was observed. The employment of nano-scale PAN fibres as a carrier allowed to provide a stable settlement of nano-scale TiO_2 particles; however, the usage of water in the spinning solution did not yield the expected results, consistent with the results presented in the paper [16], i.e. an increased porosity of PAN fibres. The presence of nano-scale titanium oxide particles boosted the viscosity of the PAN/DMF/H_2O/TiO_2 spinning solution, thus a lack of continuity was observed in the electrospinning process. Despite the lack of porosity, the obtained nano-scale fibres, containing nano-scale fibres in the amount of 2% and 3% featured a high photocatalytic efficiency.

J. S. Im et al. [17], similarly to Prahsarn, with the use of electrospinning method, spun nano-scale composite fibres in a polyacrylonitrile matrix containing titanium dioxide particles. However, he increased the TiO_2 mass concentration up to 10% relative to the mass of the entire solution, with the final mass composition of PAN:DMF:TiO_2 solution being 1:9:1. In the process of spinning nano-scale composite fibres, constant parameters were employed, among others: distance between electrodes amounting to 10 cm, applied voltage between electrodes amounting to 15 kV and spinning solution flow rate amounting to 1.5 ml/h. J. S. Im, in the course of conducted research, employed a drum collector, rotating with a constant angle speed of 300 rpm — contrary to the already mentioned papers [14–16], which described processes in which flat collectors had been employed. The process of electrospinning resulted in nano-scale composite PAN fibres/nano-scale TiO_2 particles, with diameters reaching 800 nm. On the basis of an analysis of the spun fibres, conducted with the use of SEM imaging, a tendency to generate agglomerates of the used nano-scale particles within the volume of the nano-scale fibre was established. The diameters of the resulting agglomerates of titanium oxide particles reached 50–100 nm, with a tendency of reinforcement phase coagulation being explained as a result of the presence of electrostatic interaction. Positively charged TiO_2 particles were to interact with Coulomb's force with positive charges accumulated on the surface in the path between the needle and the nano-scale fibre collector, which resulted in forcing them inside the fibres. But this explanation is erroneous, which is proved by visible agglomerates of nano-scale particles in composite fibres obtained by the J. S. Im's research team. If nano-scale particles would feature monomial positive charges, then according to Coulomb's law, they should interact electrostatically with each other with a repulsive force. This fact is contrary to the possibility of particle agglomeration. If the hypothesis of the authors of the paper [17] is just, then an SEM analysis would indicate the presence of nano-scale particles inside the entire volume of fibres in a polyacrylonitrile matrix, wherein nano-scale TiO_2 particles would not agglomerate, but would be evenly dispersed within the fibres.

In their paper, J. P. Jeun et al. [18], similarly to J. S. Im in paper [17], employing the electrospinning method, generated nano-scale polyacrylonitrile fibres containing nano-scale titanium

oxide particles from PAN/DMF/TiO_2 spinning solution with mass proportions amounting to, respectively, 1:9:1. Nano-scale TiO_2 particles were obtained with the employment of sol-gel process, and their diameters reached 80–300 nm. The employment of a flat collector and constant solution parameters — among others: solution flow rate amounting to 2 ml/h, distance and the potential difference between electrodes amounting to, respectively, 6 cm and 15 kV — made it possible to obtain nano-scale polymer PAN and composite PAN fibres/nano-scale titanium oxide particles. Fibres generated with the use of 10% polyacrylonitrile solution in dimethylformamide featured a lack of structural defects and constant diameter values along the entire length of the fibres that amounted to 100 nm. Addition of 10% mass of nano-scale TiO_2 particles to the spinning solution resulted in a ten-fold increase in the diameters of the obtained nano-scale composite PAN/TiO_2 fibres relative to pure PAN fibres obtained with the employment of the same process parameters. The spun nano-scale composite fibres featured diameters of 1 μm, plus there was no phenomenon of reinforcement phase agglomeration observed. This fact may be explained by relatively large diameters of the used nano-scale particles, thus adhesive forces per unit of particles' area were smaller than in the case of other described papers [14–16].

Byung Chul Ji et al. [19] spun nano-scale composite PAN/TiO_2 fibres using the following electrospinning process parameters: distance and difference of potentials between electrodes amounted to, respectively, 15 cm and 15 kV. There was, however, no information in the paper about the employed spinning solution flow rate in the process of electrospinning. As a reinforcement phase for nano-scale fibres, Ji used nano-scale titanium oxide particles with diameters of 30 nm, based on 10% (mass) polymer solution in dimethylformamide he created a number of mixtures containing titanium oxide with the following PAN/TiO_2 ratios: 1:0, 1:1, 1:2, and 1:2.5. Surface topography analysis of the obtained polymer and composite nanofibres conducted with the use of a scanning electron microscope indicated that diameters of fibres obtained out of pure polyacrylonitrile averaged to 100–500 nm, with the most numerous group having features of nanofibres with diameters of 300 nm. A 50% mass share of nano-scale particles relative to polymer's mass did not add to changes in morphology of the obtained fibres. In this case, the diameters of fibres amounted to 100–500 nm, with the most numerous group of nano-scale fibres featuring diameters of 300 nm. The employment of a spinning solution with PAN/TiO_2 ratio of 1:2 resulted in a considerable rise in the diameters of the observed nano-scale composite fibres. For these materials, the diameters of fibres reached 200–700 nm, and the most numerous were fibres with diameters of 600 nm. The employment of a solution with the highest mass concentration of nano-scale titanium oxide particles relative to polymer's mass, amounting to as much as 71%, caused a subsequent increase in diameters of the obtained nano-scale fibres. In this case, diameters reached the range of 300–700 nm, and the most numerous were the fibres with diameters of 700 nm. The nano-scale composite PAN fibres/nano-scale TiO_2 particles were characterized by numerous structural defects in the form of the so-called 'fusiform beads', i.e. a lack of a constant diameter along their entire length.

In their paper [20], the team from the United States, led by Liwen Ji, conducted an analysis of the influence of the mass concentration of nano-scale silicon particles and the voltage applied between electrodes during the electrospinning process on the morphology of the obtained nano-scale PAN/SiO_2 fibres. The basis of preparation of spinning solutions was 5% (mass) PAN polymer solution in dimethylformamide, containing nano-scale silica particles in mass concentrations relative to the polymer amounting to, respectively, 0%, 1%, 2%, and 5%. The diameters of the used particles amounted to ca. 7 nm, which already at the production stage of spinning solutions generated a strong tendency of reinforcement phase coagulation, which agglomerated to diameters of 80 nm. The obtained spinning solutions were subjects of the electrospinning process, under constant process parameters, among others: solution flow rate amounting to 0.5 ml/h and distance between electrodes amounting to 15 cm. A variable parameter, amounting to, interchangeably, 14 kV, 16 kV and 18 kV was the difference of potentials applied between the nozzle and the collector. In the case of all obtained samples, the diameters of nano-scale fibres reached the range of 100–400 nm, with, both, the concentration of the employed nano-scale silica oxide particles and the potential difference between electrodes employed during electrospinning process were of substantial influence on the

presence of structural defects of the spun fibres. With 14 kV voltage, only nano-scale fibres obtained with the use of pure spinning solution were lacking structural defects in the form of beads. With the increase in the SiO_2 mass concentration in the spinning solution, both, an increase of diameters of the obtained nano-scale fibres, as well as an increase of the number of structural defects in the form of fusiform and spherical beads were observed. A similar tendency to change in the diameters of nano-scale fibres and an increase in the number of their structural defects were observed with 16 kV range voltages. However, in this case, the obtained nano-scale fibres featured more homogeneous surface and constant diameter values along their entire length. Defects in the form of scarce fusiform beads were present only in the case of fibres obtained from spinning solutions containing a mass volume of 2% and 5% of nano-scale silicon oxide particles relative to polyacrylonitrile's mass. Similar results were obtained with the employment of higher voltages applied between the nozzle and the collector, i.e. 18 kV. In the case of this sample, the obtained nano-scale fibres featured, in turn, greater diameters relative to samples obtained with the employment of lower voltages, amounting to, respectively, 16 kV and 14 kV.

Liwen Li with Xiangwu Zhang, concurrently with researches presented in their paper [20] conducted researches covering repeated experiments with the use of the same spinning solutions, i.e. 5% (mass) polyacrylonitrile solution in dimethylformamide, containing nano-scale silicon oxide particles in the amounts of, respectively, 0%, 1%, 2%, and 5% of mass concentration of silica relative to polymer's mass [21]. In the paper [21], just one value of the voltage between the electrodes was employed, i.e. 16 kV; at the same time, the spinning solution feed rate in a nozzle was not provided. Most likely, the selection of these process parameters was a logical consequence of results presented in the paper [20], in which nano-scale fibres featuring the smallest number of structural defects were obtained when 16 kV voltage was employed. Also, in this case, similarly to researches that Li presented with his team in the paper [20], the nano-scale fibres featured constant diameter values along their entire length, and the values range was 200–30[illegible].

A year later, L. Ji with Z. L. Medford and [illegible]g in their paper [22], using 7% (mass) PAN solution in DMF, containing nano-scale silicon oxide particles in the amounts of, respectively, 0%, 5%, 10%, and 20% of mass silica concentration relative to polymer's mass obtained nano-scale PAN/SiO_2 fibres using electrospinning method. In the case of those researches the following parameters of the electrospinning process were applied: solution flow rate in the amount of 0.8 ml/h, distance and the potential difference between electrodes amounting to, respectively, 15 m and 21 kV. There were, however, no morphological analysis results of the obtained fibre materials, and the obtained nano-scale fibres were subsequently subjects of carbonisation process in order to degrade polymer phase and obtain nano-scale carbon fibres characterised by high porosity.

In 2014, Na Wang et al. described the process of manufacturing and morphological analysis of the obtained composite PAN/SiO_2 fibres. Spinning solutions constituted two types of polyacrylonitrile mixtures in dimethylformamide, containing, respectively, 6% and 12% of polymer's mass [23]. To such mixtures nano-scale silicon oxide particles were added, corresponding to 0%, 4%, 8%, and 12% of the mass concentration of particles relative to the mass of the used polyacrylonitrile. Analysis of surface topography of the spun PAN polymer and PAN/SiO_2 composite fibre mats, conducted on the basis of the surface imagining in scanning electron microscope showed a considerable increase in the diameters of the obtained fibres, up to ca. 130 nm for fibres not containing nano-scale silica particles, and up to even 800 nm for fibres with the highest, 12% concentration of nano-scale particles. On the surface of the spun nano-scale composite fibres, numerous agglomerates of the used reinforcement phase were observed, which clearly stems from nanometric diameters of silica particles that fall within the range of 7–40 nm.

Subject literature contains no references of the influence of nano-scale bismuth oxide (Bi_2O_3) particles as a reinforcement phase for polymer fibres. Nevertheless, due to their characteristics — covering among others and especially: optical constants (high refraction coefficient of light and high value of permittivity), wide energy separation and photoluminescence and photoconductivity capacities — this oxide may successfully replace widely used titanium oxide and serve the purpose

of building such devices, like fuel cells, gas sensors, optical layers for optoelectronics, photovoltaic cells, high-temperature superconductors and functional ceramics [24–27].

A wide-spectrum literature study conducted within the scope of this paper, covering the field of optical characteristics of the polymer and composite nanofibres obtained by electrospinning method proved that, as of now, there have been no attempts to devise a method for determination of optical constants for this type of materials. Up to the present, researches on optical characteristics of nano-scale polymer or composite fibres concentrated on merely a description of characteristics of absorbance/transmittance spectra as a function of wavelength, which were obtained for the analysed fibres using UV-Vis spectroscope [28–32]. Additionally, based on the obtained spectra $A(\lambda)$, the widths of energy separations were determined for thin spun strata consisting in nano-scale fibres [32–36]. On 1 November 2017, a single paper was published, covering the analysis of optical constants of electrospun nano-scale fibres, based on the spectroscopic ellipsometry technique [37]. In that paper, Richard Galos et al. proposed and devised the already mentioned theoretical stratified model for piezoelectric nano-scale PZT fibres, obtained with the method of electrospinning from a solution.

Figure 1 presents a comparison of stratified models used for analysis of optical constants for solid PZT stratum (Fig. 1) and nano-scale PZT fibres (Fig. 1). In the case of a flat mat stratum, consisting in nano-scale PZT fibre, there were three resultant strata introduced: 10 nm PZT stratum coupled with silicon oxide on a silicon wafer, 400 nm PZT stratum including (according to Effective Mean Approximation method — EMA) 60% of free space between single fibres, and 50 nm stratum, including surface coarseness of the fabric.

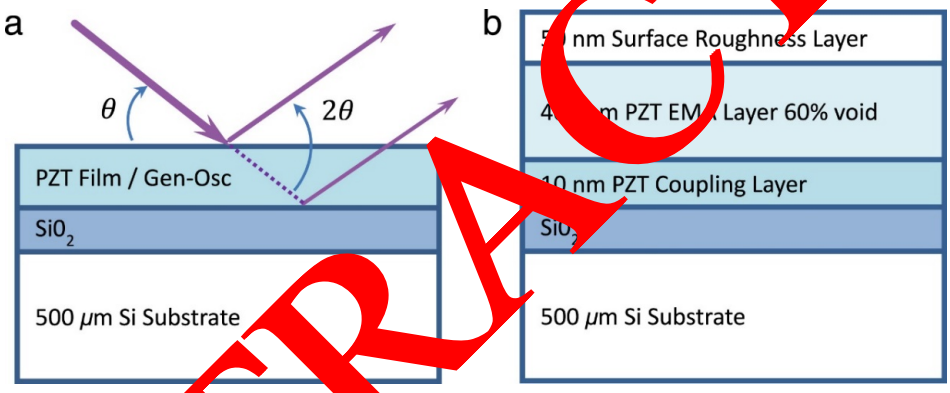

Fig. 1. Stratified model used by Richard Galos for the analysis of optical constants: a) solid PZT stratum on a silicon wafer; b) fibrous stratum consisting in nano-scale PZT fibres [chart adapted from paper [43], by the first author's permission].

The development of a stratified model also required the employment of atomic force microscope (AFM) in order to analyse the geometry and condition of surface coarseness of the examined fibrous stratum. Galos team employing the Effective Mean Approximation (EMA) and AFM topographical analysis of the surface, in order to determine the stratified model, being a resultant of a porous and fibrous PZT mat, which. The obtained results used during researches with the use of the ellipsometric spectroscopy technique in the final outcome allowed for determination of actual and imaginary portion n and permittivity ε of the examined PZT fibres.

The method of determination of optical constants for electrospun nano-scale fibres described in the paper [37] requires complex and expensive research equipment, e.g. atomic force microscope and ellipsometric spectroscope. In addition, this method is time-consuming and measurements of the fabric surface condition and running modelling of individual strata, resulting from the fibrous mat morphology, clearly influence the increase in the possibility of measurement errors and a decrease in accuracy of final results for optical constants for the analysed fibres.

Materials and Methods

In order to prepare the spinning solution, the following were used: polymer, polyacrylonitrile (PAN purity of 99%, Mw = 150 000 g/mol). The reinforcing phase was successively comprised of nanoparticles of SiO_2 (99% purity, particle size of 12 nm), nanoparticles of TiO_2 (purity 99%, particle size of 10-20 nm) and nanoparticles of Bi_2O_3 (purity 99%, particle size of 90-200 nm). The solvent was *N,N*-dimethylformamide (99.8% purity). The final products were solutions of DMF/PAN/nanoparticles (sequentially TiO_2, Bi_2O_3, SiO_2) at a concentration of 5% by weight, sequentially: 0, 4, 8 and 12% concentration of nanoparticles by weight. In order to break the agglomerates of the reinforcing phase, a measured amount of nanoparticles was added to *N,N*-Dimethylformamide, and so the prepared solutions were subjected to sonification for 1 h, automatically filling the evaporating solvent. Immediately after the process of sonicati[illegible]asured amount of polymer was added to the solution and subjected to mixing using a magnetic mixer [illegible]r 24 hours at room temperature. Immediately after mixing, the solution was placed in a [illegible]mp devi[illegible] - a sterile syringe. Polymer nanofibres were obtained using the electrospinning m[illegible]d fr[illegible]the sol[illegible]tion using the device FLOW - Nanotechnology Solutions Electrospinner 2.2.0-5[illegible]00. In the elec[illegible]spinning process, under the influence of potential difference applied between the no[illegible]e and the c[illegible]llector, there is an electrostatic field generated, which, in turn, cause the charges to indu[illegible]n the [illegible]rface of the spinning solution flowing from the nozzle. Under the influences o[illegible]he electros[illegible]field intensity, a drop of solution in the nozzle's opening is deformed and assu[illegible]es a [illegible]ical shap[illegible] (so-called Taylor cone), which is accompanied by a relocation of charges tow[illegible]ds the gr[illegible]ded collector. The flow of the spinning solution towards the collector will be ini[illegible]ated after the c[illegible]ical value of current is exceeded, and then, under the influence of the applie[illegible] electrostatic field between electrodes, the spinning solution's liquid is stretched to the form of a th[illegible]fibre. Whe[illegible] the stream diameter decreases, the stream area to volume ratio increases. The solvent eva[illegible]ates, a[illegible]d the spinning solution solidifies to the form of polymer fibre, which subsequent[illegible]diments o[illegible]the collector's surface. The employed parameters of the electrospinning process were p[illegible]esc[illegible]d in Table 1.

The constant process parameters were as [illegible]llows: s[illegible]lution flow rate, voltage applied between the nozzle and the collector, and dur[illegible]of the p[illegible]ocess. Finally, 4 groups of materials, which are fibrous mats, were obtained, i.e.:

1. PAN polymer nanofibres,
2. PAN composite nan[illegible]ibres in t[illegible]polymer matrix reinforced with nanoparticles of TiO_2 with a mass concentrati[illegible]f 4%, 8% a[illegible]12%, respectively,
3. PAN composite nanofi[illegible]s in the polymer matrix reinforced with nanoparticles of Bi_2O with a mass conc[illegible]ntration of 4[illegible]8% and 12%, respectively,
4. PAN com[illegible]posite nanofibres in the polymer matrix reinforced with nanoparticles of SiO_2 with a mass co[illegible]ntration of 4%, 8% and 12%, respectively.

All of these [illegible]oups o[illegible] materials are made for two different configurations of the distance between the [illegible]ctrodes [illegible]2.5 cm and 20 cm, respectively, which allowed to expand the study area to 20 [illegible]duce[illegible] samples.

[illegible]le. 1. The electrospinning process parameters used during obtained nanofibers.

Fixed parameters of the electrospinning process	
Parameter	**Value**
The flow rate of the solution, p [ml/h]	0.7
Potential difference between the electrodes, U [kV]	19
The duration of the process, t [min]	7
Variable parameters of the electrospinning process	
Parameter	**Value**
Distance between the electrodes, d_1 [cm]	20
Distance between the electrodes, d_2 [cm]	12.5

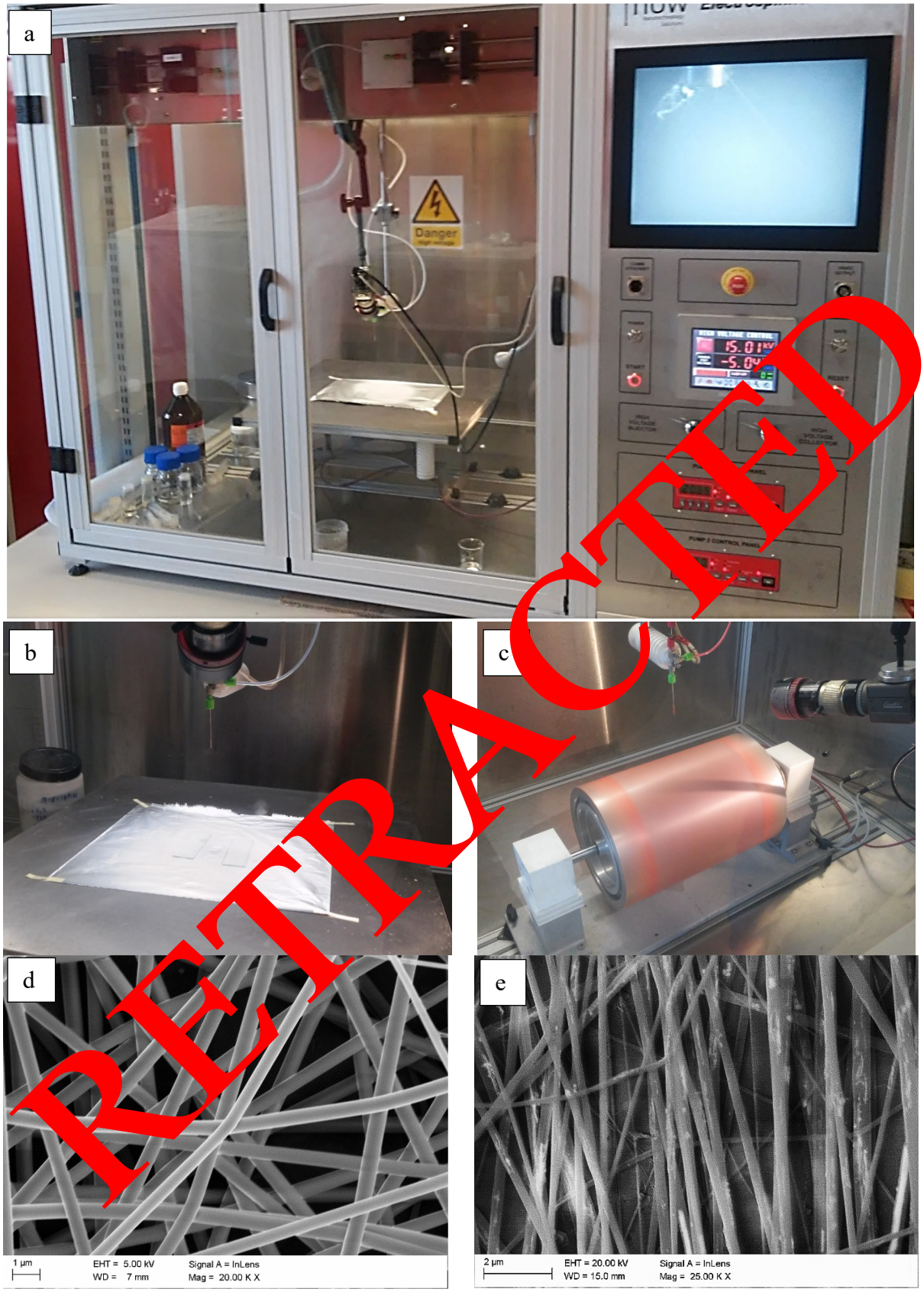

Fig. 2. a) station for generation of nano-scale polymer and composite fibres: FLOW – Nanotechnology Solutions Electro spinner 2.2.0-500; b, c) in succession, flat and drum collector, which allow to obtain: d) nano-scale fibres with random arrangement; and e) nano-scale oriented fibres (own research).

In order to identify the composition and morphology of the reinforcing phase, an X-ray analysis and a structural analysis of the applied ceramic nanopowders were carried out. The X-ray studies of the analysed materials were carried out on the X-ray X'Pert Pro diffractometer of the Analytical Company. The measurement was performed with the step wise method (in steps of 0.026 degrees and a step time equal to 30 seconds) in Bragg-Brentano geometry using the axis of the beam deflected of the detector PIXcel 3D. Filtered radiation of the lamp with the cobalt anode ($\lambda K\alpha$ = 0.17909 nm), supplied with a voltage of 40 kV at a current of glowing of 30 mA, was used. When solving the obtained diffractograms, a dedicated database of PAN - ICSD files was used. The resulting polymer composite nanofibres were subjected to quantitative and qualitative analysis using EDX X-ray microanalysis, and imaging of the surface topography using the scanning electron microscope Zeiss Supra 35, with the X-ray spectrometer Trident XM4 supplied by EDAX. Based on the SEM photographs, zoomed 50 000 times, the diameters of the randomly selected nanofibres were measured using the DigitalMicrograph program, and then their mean value and the chemical composition based on EDX spectra were specified. In order to study the properties of the obtained optical fibrous polymer and composite layers, the nanofibres were applied on a silicon substrate, and then subjected to ellipsometry analysis.

The study involved selected fibres produced with a greater distance separating the nozzle and the collector of d_1 = 20 cm, due to the fact that the fibrous mats obtained with this parameter of the electrospinning process were characterised by a much lower average of the finished thickness than those produced when using the distance between the electrodes equal to d_2 = 12.5 cm, which significantly influenced the improvement of quality measurements of the refractive index n, the extinction coefficient k, the real and imaginary part of dielectric constant ε of the obtained materials. Ellipsometry measurements of the prepared samples, which were the nanofibres applied on the silicon substrates, were carried out using the Sentech SE 850 E ellipsometer in the wavelength range of 240-2500 nm. The device was controlled by the SpectraRay 3 software. The measurements of ψ and Δ were carried out at a constant falling light angle of 70°. The value of the thickness of the obtained polymer and the composite mats was less than 1 μm, which guarantees that the results of the carried out ellipsometric and UV/VIS analyses are characterised by high accuracy and low error.

In order to analyse the optical characteristics of thin strata, the spectroscopic ellipsometry technique is widely used. This method is based on analysis of changes in the polarisation of light beam following its reflection from the analysed surface. The results of optical analyses are precise and reliable only when the analysed stratum is perfectly flat and parallel, i.e. when it is perfectly even. If a stratum is coarse, the obtained ellipsometric spectrum brings information of not only optical characteristics of the analysed sample, but also of the surface condition, thus the obtained optical constants values are erroneous. In order to avoid measurement errors connected with stratum's coarseness, the so-called theoretical stratified optical model is used, in which — besides the stratum being the actual sample — there is additionally a homogenous stratum representing the resultant optical constants of the material, which the analysed stratum is made of, as well as the surrounding conditions (gas, e.g. air), which is present in the sample's pores [38]. This method boils down to the interpretation of the coarse stratum as a composite material and results from the solution for the Clausius–Mossotti relation [39]:

$$\frac{\varepsilon_r-\varepsilon_h}{\varepsilon_r+2\varepsilon_h} = \sum f_a \frac{\varepsilon_a-\varepsilon_r}{\varepsilon_a+2\varepsilon_r}, \quad (1)$$

Where ε_a, ε_h and f_a represent, in succession, permittivity coefficients and volume concentration of the reinforcement phase a in the matrix material h, whereas ε_r is a resultant (macroscopic, determined with the use of spectroscopic ellipsometry) permittivity coefficient of the analysed porous/coarse stratum. In other words — determination of optical constants of the analysed stratum with the use of ellipsometric spectroscopy is, in fact, a matching of theoretical parameters of the above-mentioned stratified model, so that the modelling results would coincide with the spectra determined experimentally. This means, that if optical characteristics of a newly developed coarse stratum are to be analysed, e.g. in the form of a thin fibrous mat consisting of nano-scale polymer or composite

fibres generated in the process of electrospinning, its optical parameters must be known beforehand in order to enter them in ellipsometric analyses of the suitable theoretical stratified model. Such a model should consist in a stratum assigned to the used polymer, another stratum corresponding to nano-scale structures used as the reinforcement phase for the obtained composite material and the third homogenous stratum representing stratum's coarseness condition, optical characteristics of which are resultants of optical constants of the material the analysed stratum is made of (i.e. polymer used as a matrix and nano-scale structures fulfilling the role of the reinforcement phase) and the surrounding (gas, e.g. air) which is present in pores of the fibrous mat. The necessity to employ the stratified model induces considerable rise in consumption of time needed for the analyses, and cause this type of calculations to be erroneous, stemming from the accuracy of the developed theoretical model, i.e. accuracy of selection of optical constants of the stratum being a resultant of the coating's surface coarseness, as well as the reinforcement phases added to polymer matrix.

The method presented in this paper is a modified Swanepoel method, which, as standard, is used for determination of optical constants of solid strata. The method presented in this paper makes it possible to determine, both, the refraction coefficient of light (complex, and actual and imaginary portion), permittivity coefficient (complex, and actual and imaginary portion) of nano-scale polymer and composite fibres deposited on a glass substrate, based only on absorbance spectrum as a function of electromagnetic wavelength, registered with UV-Vis spectroscope for the analysed sample. A lack of the necessity for the introduction of the stratified model used in the case of the spectroscopic ellipsometry technique speeds up considerably and facilitates the analysis of optical characteristics of newly developed thin strata in the form of fibrous mats, consisting of nano-scale polymer and composite fibres, including semiconducting or dielectric nano-scale oxide particles. With the employment of the presented method, the knowledge of optical constants of all phases constituting a composite and of fibrous mat's coarseness condition is not required, as the data on the optical characteristics provided by absorbance spectrum of the electromagnetic radiation of the analysed nano-scale fibres, constituting a porous stratum, is a direct resultant of optical characteristics of the matrix material, reinforcement phase and morphology of the analysed stratum. Additionally, the obtained results of analyses of optical constants of the generated nano-scale fibres are not erroneous, which would stem from the necessity to use the theoretical stratified model, as is the case with spectroscopic ellipsometry method.

Absorbance measurements of the generated materials as a function of electromagnetic radiation wavelength, reaching a sample were conducted with the use of Thermo-Scientific UV/VIS Evolution 220 spectrometer. In order to analyse optical characteristics, the nano-scale fibres were deposited in the electrospinning process onto specially prepared glass substrate, in this case — microscopic slides. In order to increase the accuracy of measurements, each sample was conducted with three measurements of absorbance spectrum as a function of wavelength and on the basis of which the mean spectral characteristics were determined to be used in subsequent analyses of optical characteristics of the thin polymer and composite nano-scale fibres. Moreover, prior to the analysis of the characteristics of the generated strata, absorbance measurement for the used substrate was conducted; the resulting spectral value was subtracted from absorption spectra obtained for the fibrous strata deposited on the substrate. Subsequently, on the basis of the resultant absorption spectra, the following parameters were determined: complex refraction coefficient of light n, banded refractive index n, real n and imaginary k part of the refractive index as a function of the wavelength, complex dielectric permeability ε, as well as the real and imaginary part ε_r and ε_i of the dielectric permeability as a function of the radiation energy.

The optical analyses results, obtained on the basis of the registered absorbance spectra as a function of wavelength and with the use of a modified Swanepoel method were compared with the results of optical analyses conducted with the use of standard ellipsometry, in order to verify the correctness of the proposed method. Thickness value of the generated polymer and composite mats were less than 1 μm, and thus the necessary condition with the use of Swanepoel method was satisfied, meaning the thickness of the analysed stratum must be considerably smaller than the thickness of a substrate the nano-scale fibres were deposited on. Satisfying the above condition serves as a confirmation that the

obtained results of ellipsometric and UV-VIS analyses were characterised by a high rate of accuracy and small measurement error.

Results and Discusion

XRD analysis of nanoparticles

On the diffractogram registered for the sample with nanoparticles of TiO_2 (Fig.3), diffraction lines derived from the crystalline planes, characteristic of a rutile tetragonal structure with the space group P 42/m n m (98-008-2083 card) and the nanocrystal anatas with the space group I 41/a m d (98-015-4604 card), were confirmed. For nanoparticles of Bi_2O_3, the diffraction lines indicating the tetragonal structure of β-Bi_2O_3, with the space group P-4 21 c (98-005-2732 card), were obtained. In the case of nanoparticles of SiO_2, a wide/blurred diffraction line was observed, the so-called widening of the liquid, which is the effect of diffraction beams of x-ray radiation on the amorphous structure (Fig. 4). The angular position of the diffraction line was, according to data contained in the ICDD JCPDS database, the amorphous structure of SiO_2 (Fig. 5).

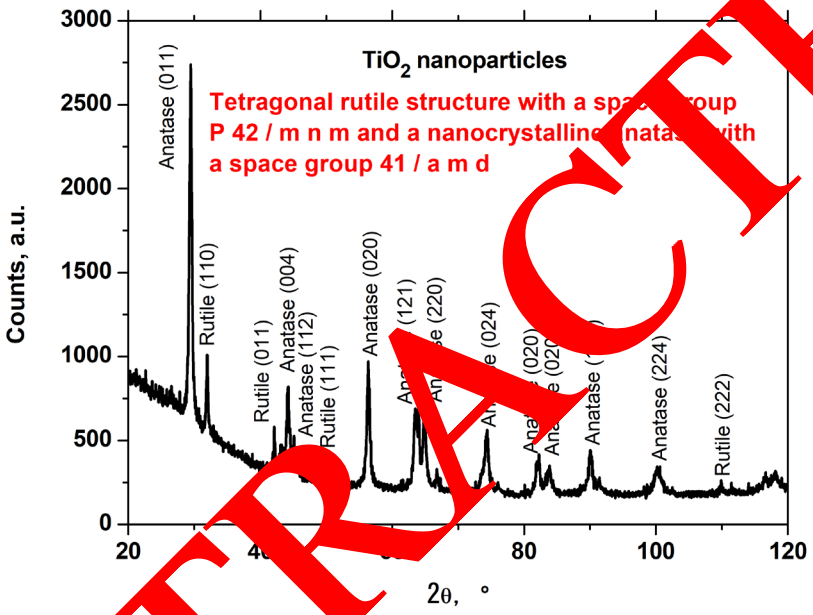

Fig. 3. XRD spectra of TiO_2 nanoparticles.

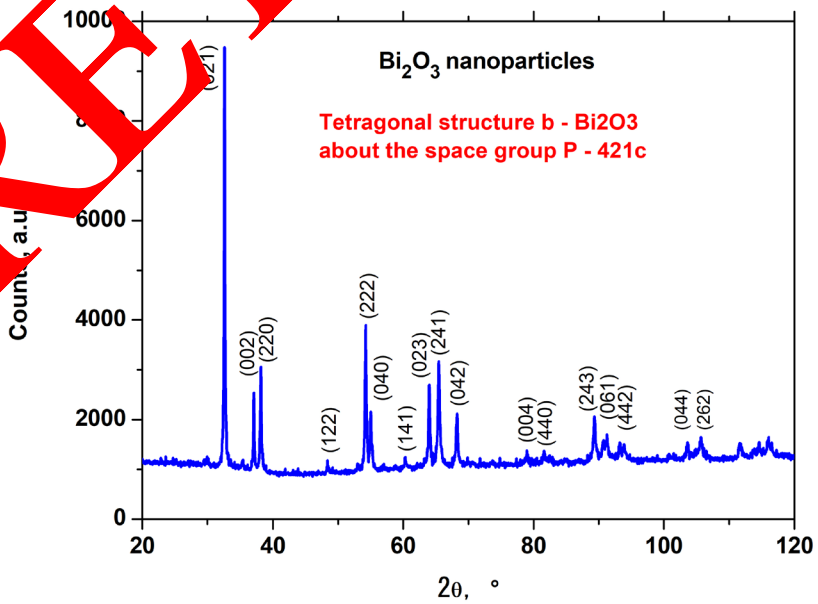

Fig. 4. XRD spectra of Bi_2O_3 nanoparticles.

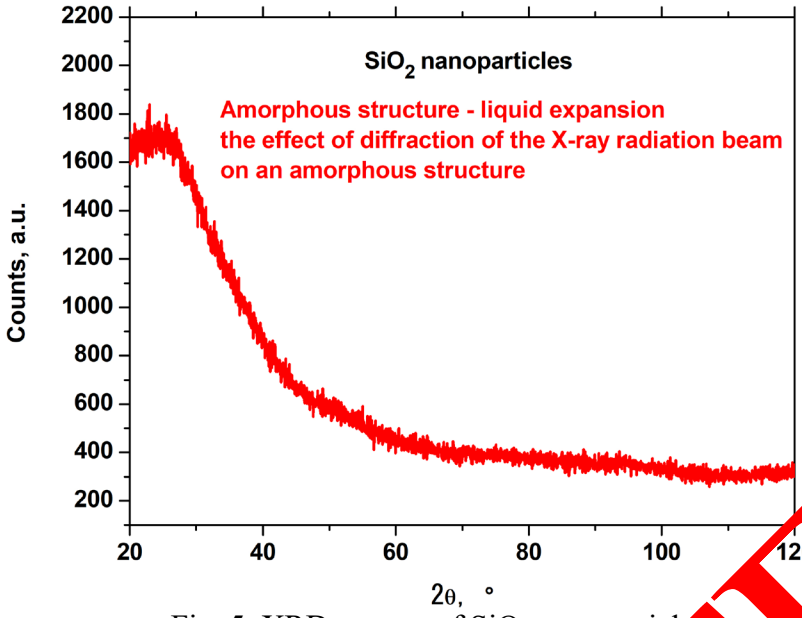

Fig. 5. XRD spectra of SiO_2 nanoparticles.

SEM and EDS analysis of nanofibers

In order to analyse the morphology and the structure of the obtained polymer nanofibres used to produce the composite fibrous materials, surface topography imaging was applied using the scanning electron microscope. An analysis of the morphology and the structure of PAN nanofibres, obtained from a solution of PAN/DMF with a concentration of 8% of polymer by weight, with the distance between the electrodes equal to 20 cm, showed that these fibres are devoid of structural defects and are characterised by a constant diameter along the entire length (Fig. 6). The fifty-time measurement of the diameters of the obtained PAN fibres showed that the measured diameters ranged from 60 to 200 nm, with the most common diameter values contained in the range of 120 to 140 nm, which represented 38% of all measured values for the diameter of the sample (Fig. 6 - the histogram).

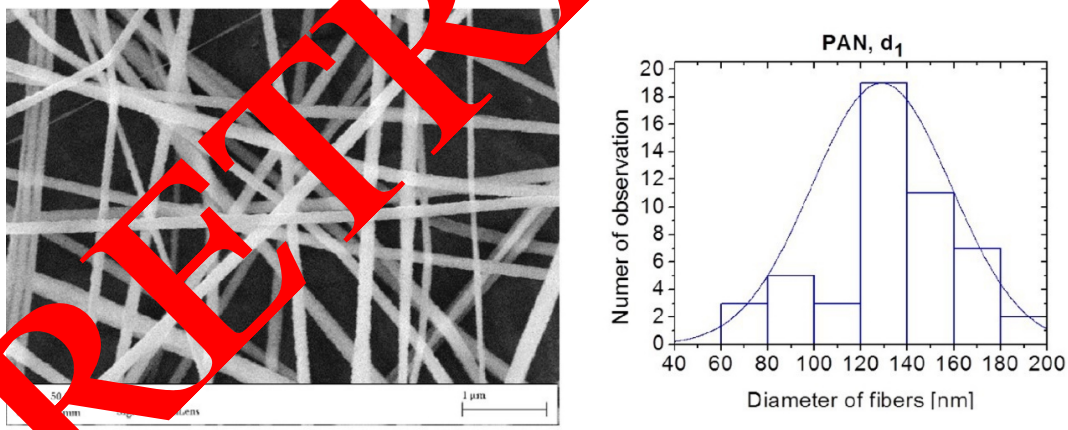

Fig. 6. SEM image of the morphology of PAN nanofibres taken at a distance of d_1 = 20 cm and a histogram showing the distribution of the measured diameters.

The study of the structure PAN nanofibre reinforced with nanoparticles of TiO_2, carried out using an SEM microscope, showed that the obtained composite fibres, unlike PAN fibres without reinforcement, are characterised by numerous structural defects, usually occurring on their surface (Fig. 6). In addition, with an increase in the concentration of the used reinforcing phases in the produced nanocomposites, an increase in the amount and the type of defects, as the heterogeneity of the fibres' morphology, was identified. X-ray microanalysis on the microareas showed that the observed defects in the nanofibres' structure in most of the analysed cases slowed down due to the local conglomeration of nanoparticles of TiO_2.which follows probably due to the presence of strong interparticle interactions between particles of the used ceramics powder. The largest number of

defects in the structure of composite PAN/TiO_2 nanofibres was observed for samples with the highest concentration of the strengthening phase, produced with a 20 cm distance between the nozzle and the collector. The measured diameter values of the composite nanofibres reinforced with titanium oxide included values in the range from 120 to 260 nm, with the largest group, representing 36% of all of the fibres of this sample, as nanofibres with diameters of 180-200 nm (Fig. 7 - the histogram).

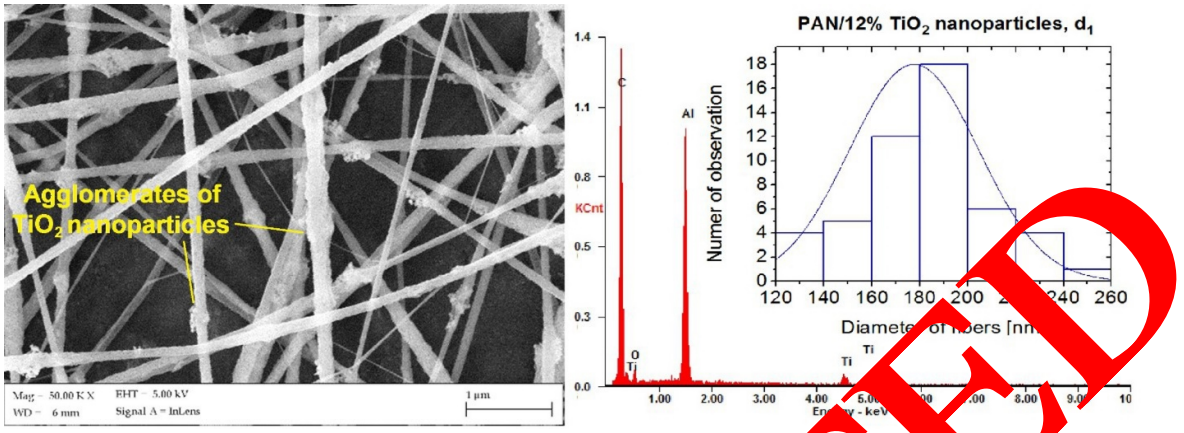

Fig. 7. SEM image of the morphology of PAN/TiO_2 nanofibres with 12% concentration by weight of nanoparticles produced at a distance of d_1 = 20 cm, with the indicated agglomerates of the nanoparticles on the fibres' surface, EDX spectre of the obtained fibres and a histogram showing the distribution of the measured diameter.

While the different nature of the fibres' morphology was identified in the case of fibrous nanocomposites reinforced with nanopowder of Bi_2O_3 with a concentration of 4%, 8% and 12% by weight, it was characterised by a uniform cross section along its entire length. The carried out studies of the morphology of composite PAN/Bi_2O_3 nanofibres and the analysis of EDX spectra showed no defects in the obtained surface structures in the form of agglomerates of the strengthening phase. However, with an increase in the concentration of Bi_2O_3 nanoparticles in a polymer to 12%, the formation of the so-called spindle-shaped beads can be seen (Fig. 8), which are structural defects of composite nanofibres, produced at a distance between the nozzle and the collector that is equal to 20 cm. The fifty-time diameter measurement showed that the diameters of the fibres from the bismuth oxide particles are in the range from 120 to 280 nm, and the fibre diameter ranging from 140 to 160 nm and from 180 to 200 nm are the largest 40% obtained group of the nanofibres (Fig. 8 - the histogram). Defects of nanofibres in the form of spindle beads and of a spherical shape belong to some of the most-common structural defects of nanofibres produced with the electrospinning method [39].

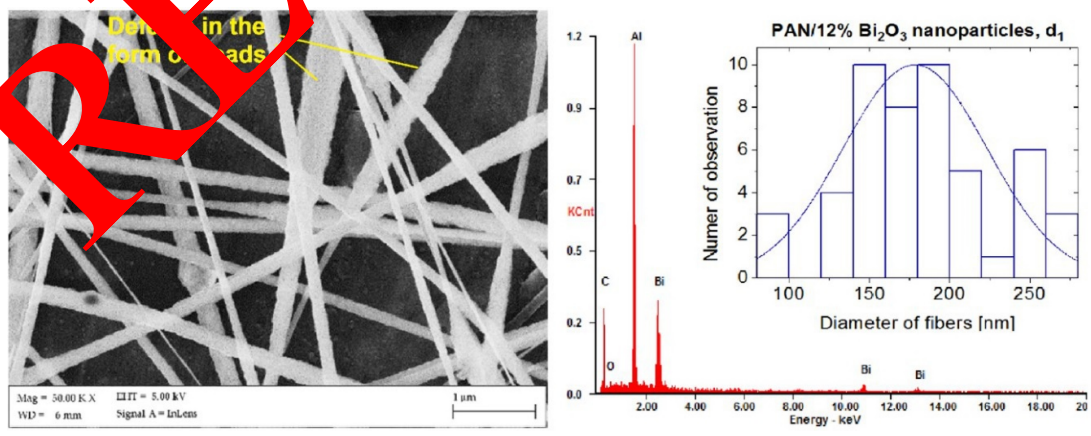

Fig. 8. SEM image of the morphology of PAN/Bi_2O_3 particle with 12% concentration by weight of nanoparticles produced at a distance of d_1 = 20 cm, with the indicated agglomerates of nanoparticles on the fibres' surface, EDX spectre of the obtained fibres and a histogram showing the distribution of the measured diameters.

An analysis of SEM images of the topography of the surface of fibrous mats, carried out with composite PAN nanofibres reinforced with nanoparticles of SiO_2, revealed the presence of a significant number of defects in the structure of the obtained nanofibres (Fig. 9). These fibres are characterised by the greatest number of defects in comparison to other produced composite nanofibres reinforced with powders of TiO_2 and Bi_2O_3. For all of the applied concentrations of the strengthening phase and the distances between the electrodes, in the case of composite nanofibres of PAN/SiO_2, both local conglomerates of nanoparticles on the surface of the fibres were observed, which was confirmed through an analysis of the EDX spectra (Fig. 9) and the defects in the form of spindle beads, which can be assessed by comparing the obtained composite nanofibres with nanofibres obtained from a pure polymer. The formation of numerous defects in the structure of the composite nanofibres reinforced with a powder of SiO_2 probably results, just like in the case of the TiO_2 powder, from the presence of strong interparticle interactions occurring between particles of the used strengthening phase, which, in turn, lead to the formation of visible agglomerates of nanoparticles. Based on the carried out SEM analysis of the surface topography of the produced fibrous mats and TEM analysis of the particle size of the used nanopowders, it can be concluded that the formation of defects in the structure of the obtained nanofibres, probably resulting from the tendency to form agglomerates of the used strengthening phase, is associated with the size of the nanoparticles. Using particles of a smaller diameter results in an increased number of defects in the structure of the obtained nanofibres. The tendency to connect nanoparticles in the agglomerates can be explained by the fact that smaller particles of SiO_2, the average value of which was equal to a diameter of 17 nm, are characterised by a much larger area of up to approx. 2 times the area of TiO_2 particles and more than 8 times larger than the area of Bi_2O_3 particles, as a result of which the forces of adhesion per mass unit, responsible for the ability to connect to the reinforcing phase in the agglomerates, are larger. In addition, the analysis of the diameters of the obtained composite PAN nanofibres reinforced with silicon nanoparticles showed that these fibres are characterised by the greatest variety of diameter values in the range from 50 to 350 nm, compared to other produced fibres (Fig. 9 - the histogram).

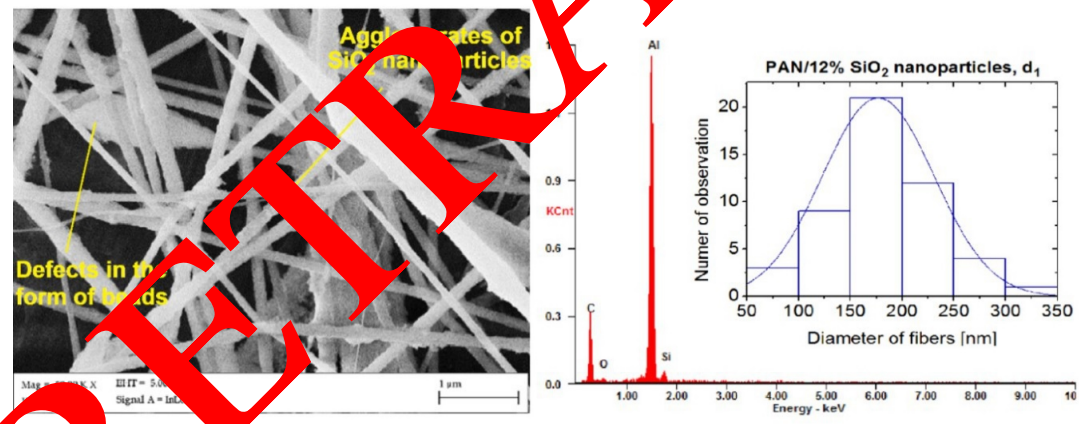

Fig. 9. SEM image of the morphology of PAN/SiO_2 nanofibres with 12% concentration by weight of nanoparticles produced at a distance of d_1 = 20 cm, with the indicated agglomerates of nanoparticles on the fibres' surface, EDX spectre of the obtained fibres and a histogram showing the distribution of the measured diameters.

The most frequently used distances between the nozzle and the collector, used during electrospinning of PAN nanofibres reinforced with ceramic nanoparticles of titanium oxide and silicon oxide, while applying a potential difference in the range of 15-21 kV, are between 10, 12 and 15 cm. The composite nanoparticles obtained based on the conditions were characterised with a diameter of 300 and 800 nm [14, 15, 11]. In order to better understand the relationship between the applicable distance between the electrodes and the diameter of the obtained fibres, we used two different distances between the nozzle and the collector, amounting to 12.5 and 20 cm, and the diameter measurement of such obtained fibres was carried out based on SEM analysis of the surface topography of the obtained fibrous mats (Fig. 9).

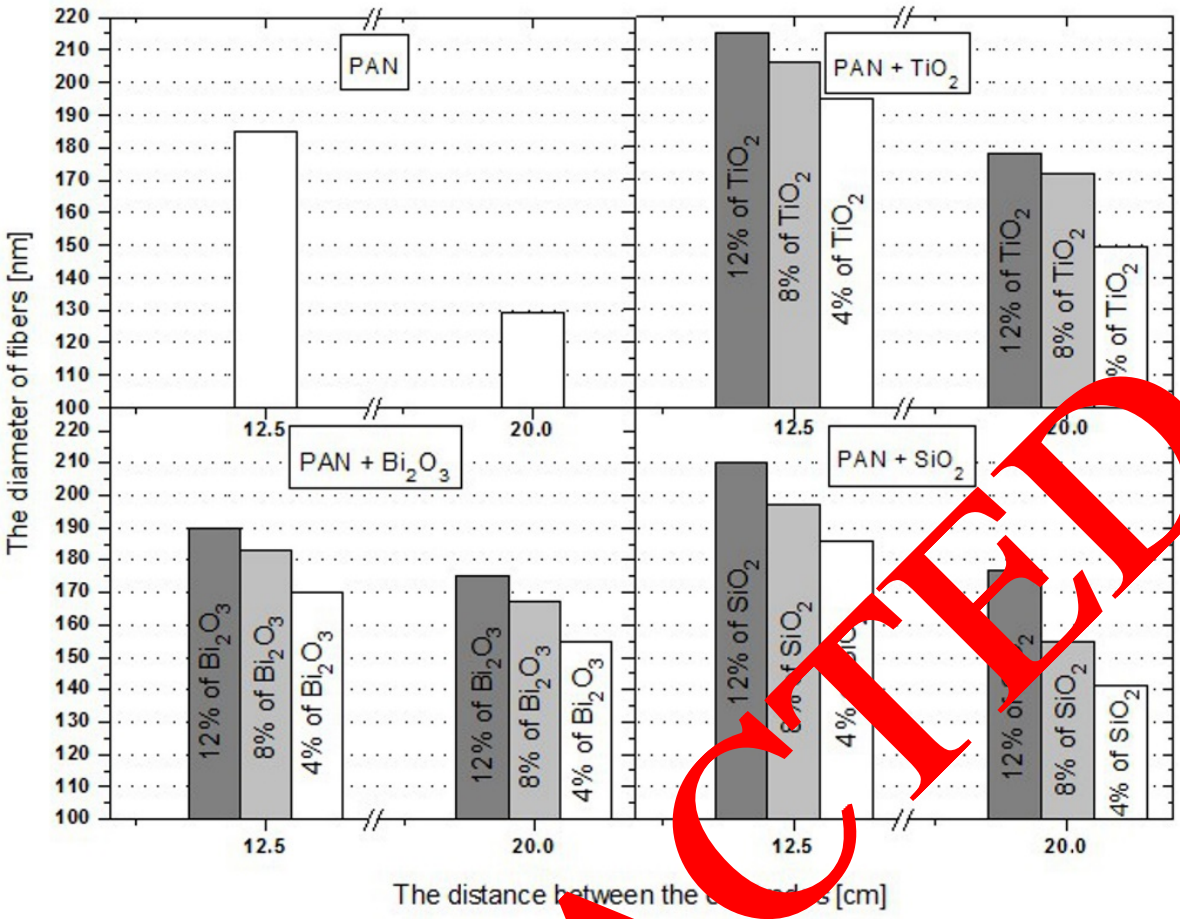

Fig. 10. Dependence of the calculated diameter of nanofibres in the function of the used distance between the nozzle and the collector for all produced samples.

In the case of a smaller distance equal to 12.5 cm, the diameter dependence of the fibres as a function of the mass concentration of TiO_2 takes the linear form, and an increase in the diameter of the obtained fibres progresses on average, 10 nm for every 4% of increase in the participation of the strengthening phase. When using nanoparticles of Bi_2O_3 as the reinforcing phase, an increase in the diameter of the nanofibres, depending on participation of the particles by weight, for both used distances between the nozzle and the collector is approximately linear (Fig. 10), with an increase of the mass concentration if Bi_2O_3 every 4% results in an increase in the diameter of the fibres, comparable as in the case of titanium oxide by approx. 10 nm. For a shorter distance between the electrodes, the diameter of the obtained nanofibres increases from 170 nm, in the case of a 4% participation of the reinforcing phase of Bi_2O_3, to 190 nm, to a concentration equal to 12%. The use of a larger distance between the nozzle and the collector contributed to an increase of the diameters of the obtained composite fibres from the value of 175 nm, corresponding to 4% of the fibres with participation of the particles of Bi2O3. For 8% of bismuth oxide concentration obtained nanofibers with 183 nm diameter, and a diameter of 195 nm, which was characterised by fibres with the highest concentration by weight of nanoparticles at 12%. In addition, in the case of PAN/SiO2 composite nanofibres, increase in their diameter accompanying the percentage participation of nanoparticles was observed, which was already observed when the remaining ceramic nanopowders were used. A change in the weight concentration of nanoparticles of SiO_2 from 4% to 12%, while a fibre with a distance of 12.5 cm equal to electrodes was produced, was associated with an increase in the diameter of the fibres, on average, by approx. 12 nm every 4% (the fibre diameter increased from 186 nm to 210 nm). Using a larger distance equal to 20 cm contributed to an increase in the diameter of nanofibres from a value of 141, for 4% concentration of silicon oxide, through 155 nm for fibres of 8% concentration of the reinforcing phase, up to 177 nm for the largest concentration of 12%. Using this distance increased the weight concentration of SiO_2 nanoparticles by 4%, causing an average

increase in the diameter of the obtained composite nanofibres by 13 nm. The observation revealed that using the reinforcing phase in the form of the ceramic nanopowders of TiO_2, Bi_2O_3 and SiO_2 added to the polyacrylonitrile significantly influenced the diameter of the composite nanofibres, compared to those obtained with the non-reinforced polymer. This is confirmed by the fact that in the case of both of the used distances between the electrodes, an increase in the reinforcing phase is accompanied by an increase in the diameter of the obtained composite fibres.

An increase in the thickness of the fibres, accompanied by a reduction of the distance between the nozzle and the collector during the process of electrospinning, both for nanofibres obtained from the non-doped PAN polymer and the composite PAN nanofibres reinforced with ceramic particles of TiO_2, Bi_2O_3 and SiO_2, is probably caused by less power of the force acting on the induced electrical loads in the spinning solution, when the distance between the electrodes is equal to 12.5 cm, compared to the force speed that influences the induced loads at a distance of 20 cm.

The electrostatic force resulting in stretching of the polymer stream is inversely proportional to the distance between the loads gathering on the surface of the collector and the ones induced on the surface of the solution that drop from the nozzle. Using a greater distance between the nozzle and the collector reduces the value of the force acting on the induced loads, but the actual route covered by the polymer stream along the spiral track on the section connecting the electrodes, as compared to the one covered by the beam at a distance of 12.5 cm, is much greater. This is associated with the time of the force acting on the extending polymer solution over a distance of 20 cm, which is much longer. A longer duration of action of the electrostatic force on the induced loads in the spinning mixture, and thus by a longer time of stretching the polymer stream by connecting the nozzle and the collector in the case of using a larger distance, is responsible for the formation of fibres with lower diameters.

The obtained composite PAN/SiO_2 nanofibres, while maintaining a 20-cm distance between the electrodes, are characterised by an approx. 30% smaller diameter than the ones presented herein [40], which is associated with a much larger surface. This fact means that the obtained composite mats, reinforced with silicon oxide, are a promising material that can be used to produce carbon anodes, which are used in lithium-ion batteries, after their subsequent treatment by carbonisation and chemical removal of the reinforcing phases in order to increase the porosity of such obtained carbon fibre.

As it was demonstrated by Chanyarat Pinsarn with collaborators [41], the polymer nanofibres of PAN are very good for medium in particles of TiO_2 with photovoltaic properties, providing particles with stable embedding, while preserving the large contact area of the catalyst with the reagents, thus resulting in an increase of the effectiveness of photodecomposition processes. The distance, used by the authors, between the nozzle and the collector equal to 20 cm contributed to obtaining composite PAN/TiO_2 nanofibres with diameters smaller by approx. 40%, relative to those obtained herein [41], and by 78% smaller than the diameters of composite nanofibres obtained by Ji Sun Im, Min Il Kim, Young-Seak Lee [15], and thus to a significant increase in the specific surface area of the composite mats related to receiving more efficient photocatalyst materials. It is anticipated that the composite PAN nanofibres produced by authors hereof, reinforced with Bi_2O_3 nanoparticles, due to their photocatalyst properties [37], can provide a more effective alternative to the previously produced PAN/TiO_2 nanofibres.

In addition, in the next stage of the study carried out by the authors, it is planned to examine the effects of the experimentally applied distance between electrodes, larger than the one used herein, i.e. 20 cm, on the diameter of the fibres obtained by maintaining the same parameters of solutions and the same flow rate.

Optical Analysis

Elipsometry analysis

Evaluation of thickness of the generated fibrous strata was conducted with the use of ellipsometric analysis (Tab. 2). The PAN polymer mats reinforced with nano-scale Bi_2O_3 particles featured the largest mean thickness of fibre strata, amounting to 382 nm. In the case of nano-scale TiO_2 particles

employed as the reinforcement phase, the thickness reached 296 nm and was by 10 nm larger than the thickness of a stratum obtained from nano-scale PAN fibres. The smallest fabric thickness in the case of the obtained composite fibres was observed for nano-scale SiO_2 powder, and it amounted to 262 nm, and was smaller than the thickness of a stratum obtained from pure polyacrylonitrile (Tab. 2).

Using ellipsometric analysis, measurements of coefficients of refraction of light as a function of wavelength and in the range of 250–2500 nm were conducted for the fibrous strata of nano-scale PAN polymer and PAN composite fibres, reinforced with nano-scale TiO_2, Bi_2O_3 and SiO_2 ceramic particles (Fig. 11).

The smallest value of optical permeability, amounting to 1.34 featured a stratum made of PAN polymer fibres (Tab. 3), with a value provided by the manufacturer, Sigma Aldrich, was 1.51. For all PAN composite strata/nano-scale composite particles, the obtained values of the optical permeability coefficient were higher than the refraction coefficient obtained for fibres made of polymer without admixtures.

Table 2. Results of ellipsometric measurements of the thickness of the obtained fibrous mats, spun with distances between the electrodes amounting to 20

Type of nanofibers		Thickness, nm
PAN nanofibers		286
Composite nanofibers	PAN/ 4% TiO_2	299
	PAN/ 8% TiO_2	291
	PAN/12% TiO_2	298
	PAN/ 4% Bi_2O_3	383
	PAN/ 8% Bi_2	380
	PAN/ 12% Bi_2O	382
	PAN/ 4% SiO_2	263
	PAN/ [illegible] SiO_2	272
	P[illegible]/ 12% SiO_2	250

Adding nano-scale TiO_2 particles with a mass concentration of 4% to polymer fibres spurred an increase of the refraction coefficient of light up to 1.55, and a subsequent increase in the content of nano-scale TiO_2 filling resulted in an increase in the optical density (considered here as a capacity of the analysed material medium to decrease the speed of propagation of electromagnetic radiation relative to the speed of radiation propagation in vacuum) of fibrous PAN/TiO_2 composite mats, which is evidenced by determined coefficients of refraction of light for subsequent concentrations. For the concentration of 8% the obtained optical permeability value amounted to 1.68, whereas for the maximum concentration of nano-scale particles it equalled 1.73.

Addition of nano-scale Bi_2O_3 particles in the amount of 4% mass to a polymer effected in an increase of the refraction coefficient of light from 1.34 for a pure polymer up to 1.46. The increase of the concentration of nano-scale bismuth oxide particles in nano-scale PAN composite fibres/nano-scale Bi_2O_3 particles up to the value of 8% and 12% conditioned another increase of the refraction coefficient of light for the obtained nano-scale composites up to, respectively, 1.55 and 1.8. The smallest increase in optical permeability relative to remaining composite strata was obtained with the use of nano-scale SiO_2 particles. The employed concentration of nano-scale silicon oxide particles, amounting to 4% mass relative to polymer's mass conditioned an increase of the refraction coefficient of light by 0.02 relative to the determined coefficient for a pure polymer, whereas for 8% content of nano-scale SiO_2 particles the optical permeability equalled 1.39. The highest value of the refraction coefficient of light — in the case of nano-scale SiO_2 particles — was obtained for 12% mass concentration of the reinforcement phase, which in this case equalled 1.5.

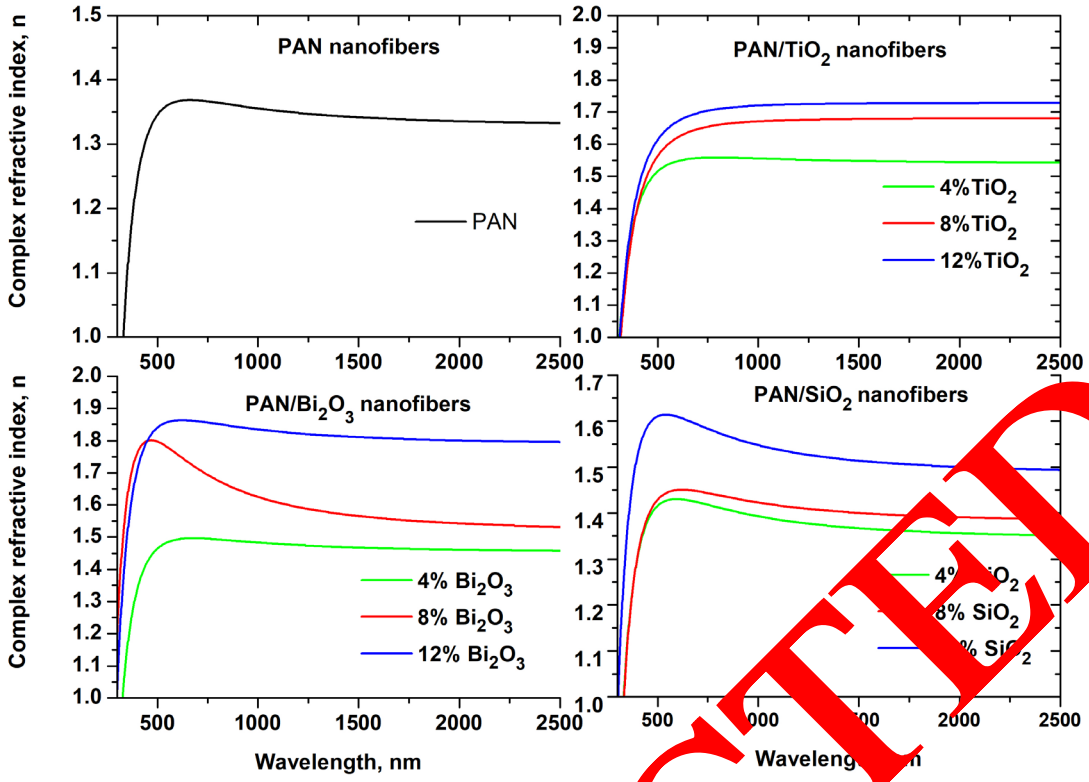

Fig. 11. Results of ellipsometric measurements of coefficients of refraction of light for the obtained fibrous strata, generated with distances between electrodes amounting to 20 cm (values given for wavelengths of 1800 nm)

Table 3. Results of ellipsometric measurements of coefficients of refraction of light for the obtained fibrous strata, generated with distances between electrodes amounting to 20 cm (values given for wavelengths of 1800 nm).

Type of nanofibers		Refractive index n
PAN nanofibers		1.34
Composite nanofibers	PAN/ 4% TiO_2	1.55
	PAN/ 8% TiO_2	1.68
	PAN/12% TiO_2	1.73
	PAN/ 4% Bi_2O_3	1.46
	PAN/ 8% Bi_2O_3	1.55
	PAN/ 12% Bi_2O_3	1.8
	PAN/ 4% SiO_2	1.36
	PAN/ 8% SiO_2	1.39
	PAN/ 12% SiO_2	1.5

For all of the groups of the produced composites reinforced with ceramic powders, an increase in the refractive index accompanying an increase in the participation of the mass concentration of the reinforcing phase was observed. The lowest increase in the *n*, obtained for composite PAN nanofibres reinforced with nanoparticles of SiO_2, is due to the relatively low value of refractive index of the used ceramic reinforcement that varies in the range of the visible waves a ± 1.45. Both, the used polymer and the particles of SiO_2, have a similar *n*, i.e. the mechanism of interaction of electromagnetic radiation with these materials and the composites obtained with their participation is similar, as evidenced by the results of studies of the optical properties. The refractive index values obtained for composites of PAN reinforced with titanium oxide and bismuth oxide are similar. This is due to the relatively small difference between the refractive index, for TiO_2 approx. 2.6 and for Bi_2O_3 approx.

2.5 respectively, suggesting much larger n of the composites produced with their participation compared to materials reinforced with nanoparticles of SiO_2.

The dependence of the dielectric transmittance in the function of the frequency of the incident radiation on the sample can be presented in the following form [42]:

$$\varepsilon = 1 + \frac{\mu e^2}{m\varepsilon_0}\left[\frac{\omega_0^2-\omega^2}{(\omega_0^2-\omega^2)^2+\gamma^2\omega^2} - i\frac{\gamma\omega}{(\omega_0^2-\omega^2)^2+\gamma^2\omega^2}\right], \quad (2)$$

where: n is the concentration of the atoms in the sample, e and m are the loads and mass of the electron, ε_0 is the electrical transmittance of vacuum, γ is the damping coefficient, ω_0 and ω are respectively the frequency of the electron's own vibrations and electromagnetic radiation. The above equation shows that the dielectric constant is a complex value, but its real and imaginary part can be stored as:

$$\varepsilon' = 1 + \frac{\mu e^2}{m\varepsilon_0}\frac{\omega_0^2-\omega^2}{(\omega_0^2-\omega^2)^2+\gamma^2\omega^2}, \quad (3)$$

$$\varepsilon'' = \frac{\mu e^2}{m\varepsilon_0}\frac{\omega_0^2-\omega^2}{(\omega_0^2-\omega^2)^2+\gamma^2\omega^2}. \quad (4)$$

Using the relation connecting the refractive index and the dielectric constant ($n = \varepsilon^{1/2}$), for expressing the real and imaginary part of the optical transmission, takes the form of [42]:

$$n' = \left\{\frac{1}{2}[\varepsilon' + (\varepsilon'^2 + \varepsilon''^2)^{\frac{1}{2}}]\right\}^{\frac{1}{2}}, \quad (5)$$

$$n'' = \left\{\frac{1}{2}[-\varepsilon' + (\varepsilon'^2 + \varepsilon''^2)^{\frac{1}{2}}]\right\}^{\frac{1}{2}}. \quad (6)$$

The above equations show that the higher the light refraction coefficient of the studied centre, the higher its dialectic transmittance. The designated values ε (Tab.8) were provided for a wavelength of 1800 nm corresponding, as in the case of the light refraction coefficient, to stabilisation of the dielectric constant for both pure polymer fibres and fibres reinforced with ceramic nanopowders.

The obtained results match theoretical assumptions. Just like in the case of the refraction coefficient of light, the smallest value of permittivity, 1.67, was determined for strata made of pure nano-scale PAN polymer fibres (Fig. 12).

The smallest rise in dielectric constant, conditioned by the share of the reinforcement phase in the form of nano-scale ceramic powders, was observed for nano-scale SiO_2 particles. Their addition to a polymer with 2% mass concentration caused an increase in the electric permeability merely by 0.04; doubling the content of nano-scale silicon oxide particles favoured the following increase ε by 0.1 relative to the permittivity of a pure polymer.

Table 8. Results of ellipsometric measurements of an actual portion of dielectric constant for the obtained fibrous strata, generated with distances between electrodes amounting to 20 cm (values given for wavelengths of 1800 nm).

Type of nanofibers		Dielectric constant ε
PAN nanofibers		1.67
Composite nanofibers	PAN/ 4% TiO_2	2.16
	PAN/ 8% TiO_2	2.64
	PAN/12% TiO_2	2.81
	PAN/ 4% Bi_2O_3	1.94
	PAN/ 8% Bi_2O_3	2.19
	PAN/ 12% Bi_2O_3	3.07
	PAN/ 4% SiO_2	1.71
	PAN/ 8% SiO_2	1.77
	PAN/ 12% SiO_2	1.98

Addition of nano-scale SiO_2 particles with 12% mass concentration relative to the polymer to a spinning solution spurred the rise in the permittivity of the obtained nano-scale composite fibres up to 1.98. In the case of the remaining particles used, an increase of dielectric phase is also present, accompanying the increase of mass content within the reinforcement phase. Polymer reinforcement with nano-scale TiO_2 particles by 4% mass concentration favoured an increase in permittivity up to 2.16, and a subsequent increase of nano-scale titanium oxide particles mass concentration up to 8% and 12% favoured a considerable increase in dielectric constant, which, in turn, conditioned its increase up to a value equalling 2.64 and 2.81 (Fig. 12).

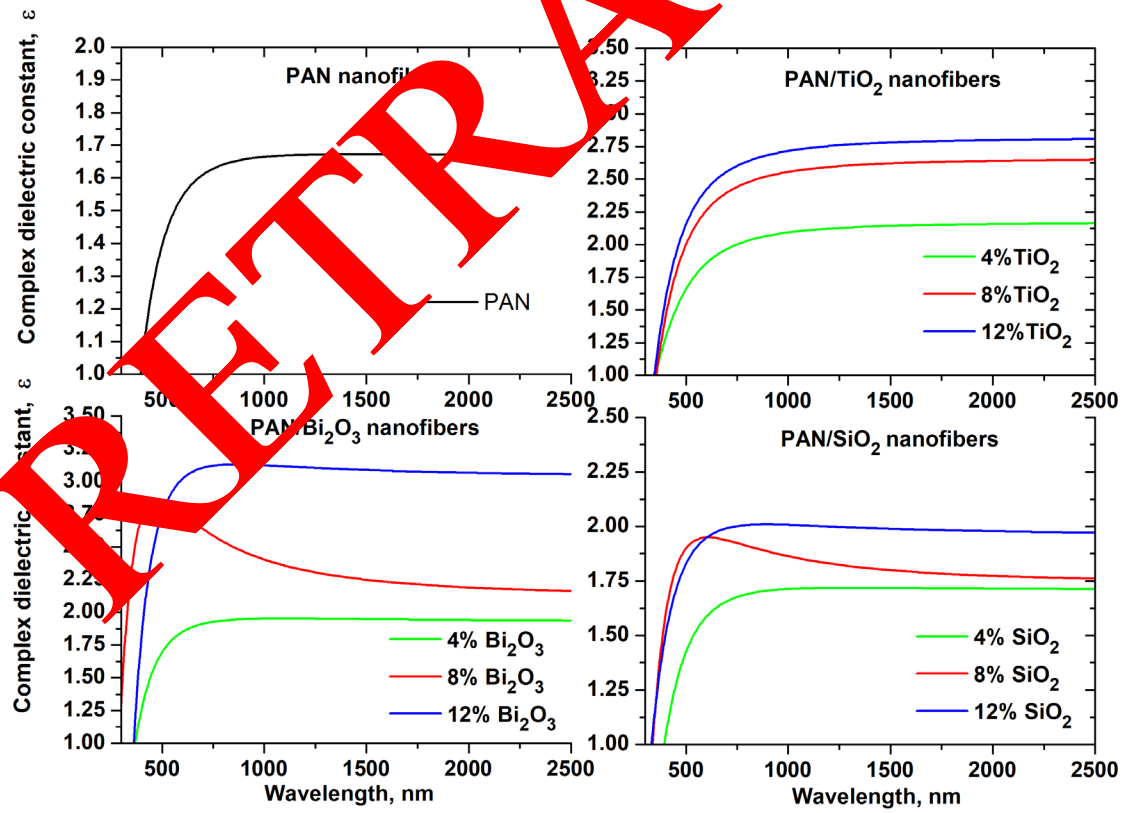

Figure 12. Dependence of permittivity as a function of wavelength for the generated fibrous strata.

The maximum value of permittivity of the analysed fibrous strata was obtained for nano-scale PAN composite fibres reinforced with nano-scale Bi_2O_3 particles. Their addition to a polymer, with 12% mass amount resulted in almost double the increase of dielectric constant relative to a value determined for a fabric made of pure polymer, reaching values of 3.07. Usage of nano-scale Bi_2O_3 particles with the lowest mass concentration in a polymer featured results similar to those obtained in the case of the employment of nano-scale SiO_2 particles with the maximum mass concentration (Fig. 52). Whereas for a fibrous stratum, reinforced with nano-scale bismuth oxide particles with a mass concentration of 8%, the determined value of permittivity constant was similar to the one obtained for fibres reinforced with titanium oxide with concentration equalling 4% and amounted to 2.19 (Fig. 12).

The conducted analyses of relative permittivity values of the generated fibrous mats coincide with theoretical assumptions, stemming from the dependence of $n = \varepsilon^{1/2}$ and the obtained ellipsometric research results for optical permeability of these materials. The increase in the mass concentration of the used nano-scale particles is accompanied by an increase in the coefficient of optical permeability, and thus with the increase of permittivity evident for every group of generated nano-scale composite fibres.

UV-Vis analysis

In order to analyse optical characteristics of the generated fibrous strata, consisting in nano-scale polymer and composite fibres, for all material groups absorbance spectra as a function of wavelength, obtained with the use of UV-Vis spectrometer were registered (Fig. 13–15). In the case of nano-scale polymer fibres, generated from 5% polyacrylonitrile solution in dimethylformamide, a sharp absorption edge was observed for radiation close to the ultraviolet band, i.e. below 350 nm (Fig. 13). Wherein, the absorption maximum corresponded with a wavelength of 320 nm, which coincides with absorption spectrum obtained for pure polyacrylonitrile by Kubala et al. in the paper [43]. This is most likely caused by electron transfers of $\pi \rightarrow \pi^*$ and $\pi \rightarrow \pi^*$ type, characteristic for organic compounds in a band close to ultraviolet. Absorption spectra registered for the obtained fibrous PAN/TiO_2 composite mats also featured a sharp absorption edge for this type of a material in a band close to ultraviolet, but the absorption maxima, irrespectively of the mass concentration of the used nano-scale titanium oxide particles matched the radiation quanta of a wavelength of 320 nm (Fig. 13). The measured absorption edges for nano-scale polyacrylonitrile fibres reinforced with nano-scale titanium oxide particles are shifted relative to absorption edges registered both for a pure polymer, as well as the reinforcement phase; absorption edge falls for wavelengths of ca. 400 nm [44]. But, with regard to a spectrum documented in the paper [44], for nano-scale TiO_2 particles there was a hypsochromic shift of materials' absorption edge towards shorter wavelengths, which most likely is a result of a presence of nitrogen atoms in polyacrylonitrile [45].

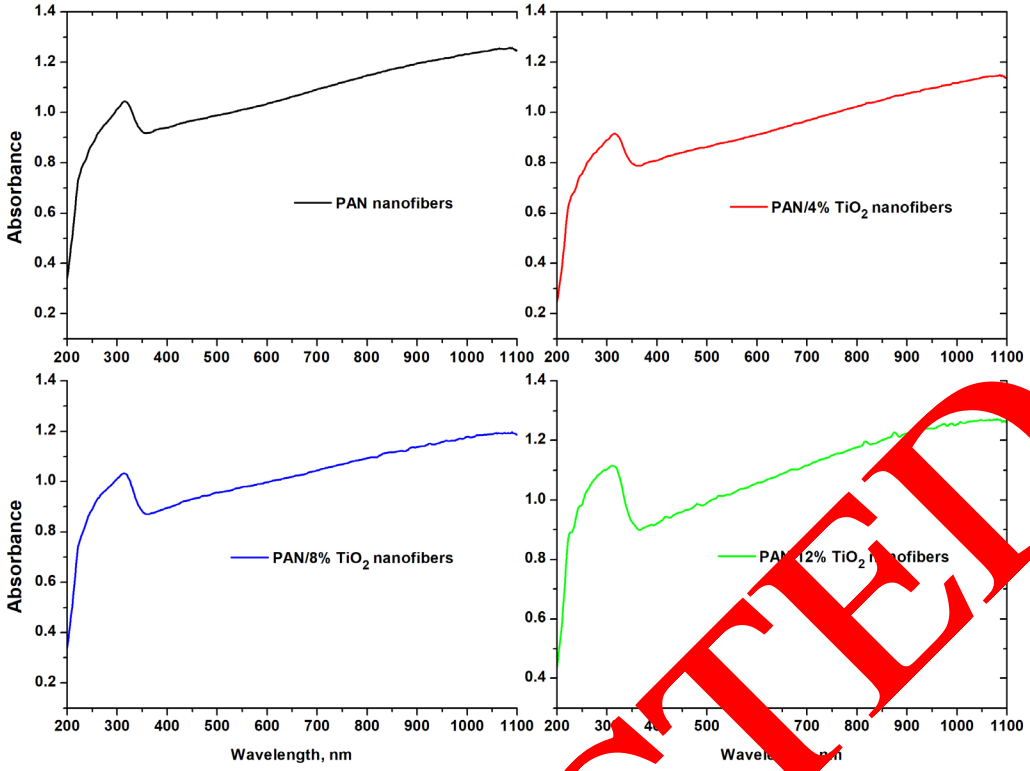

Fig. 13. UV-Vis absorbance spectra as a function of wavelength reaching the sample and obtained for nano-scale PAN fibres and nano-scale PAN/TiO_2 composite fibres.

Whereas with respect to spectrum determined for pure polymer, the increase in concentration from 4% to 12% of mass content of nano-scale TiO_2 particles in composite fibres resulted in bathochromic shift of sharp absorption edge of nano-scale PAN fibres towards nano-scale TiO_2 particle towards visible light, stemming from the presence of nano-scale titanium oxide particles, for which an absorption edge was observed already at wavelengths of 4[illegible] nm [46]. Presence of nano-scale TiO_2 powder in composite fibres caused a surge in the absorption of electromagnetic waves in a band close to ultraviolet with values of 0.1 up to 0.91 for nano-scale PAN composite/4% TiO_2 fibres and up to 1.12 for nano-scale PAN composite/12% TiO_2 fibres. The observed increase in nano-scale composite fibres' absorption of electromagnetic radiation caused by high absorption of UV radiation of the used titanium oxide (Fig. 13).

Thin fibrous strata, consisting in nano-scale PAN composite fibres containing nano-scale Bi_2O_3 particles featured optical characteristics similar to that of nano-scale PAN/TiO_2 composite fibres (Fig. 14). Also, in this case, absorbance spectra as a function of wavelengths, registered for nano-scale PAN/Bi_2O_3 fibres showed that mass content of nano-scale ceramic particles in polymer matrix had no considerable effect on the level of the observed absorption maxima, which oscillated at 1. The nano-scale PAN fibres, however, which are characterised by a gradually greater mass content of nano-scale bismuth oxide particles featured bathochromic shifts — relative to a spectrum obtained for nano-scale fibres of pure polyacrylonitrile — of sharp absorption edge towards visible light, stemming from optical characteristics of nano-scale Bi_2O_3 particles, for which absorption edge is observed in the band of visible light falling below wavelengths of 450 nm [47]. Moreover, for all fibrous mats consisting in nano-scale PAN composite fibres with 4%, 8% and 12% mass content of nano-scale bismuth oxide particles, the absorption maximum was shifted towards visible light, relative to maxima obtained for PAN/TiO_2 fibres and matched electromagnetic wavelengths of 330 nm (Fig. 13). This may evidence potentially better application possibilities of this type of nano-scale fibres, serving as photocatalytic materials in comparison to the now commonly generated and analysed nano-scale fibres with titanium oxide particles in their matrix.

Absorbance spectra as a function of electromagnetic radiation wavelength registered for thin fibrous strata, consisting in nano-scale PAN composite fibres with silicon oxide particles with 4%, 8% and 12% mass concentration relative to polymer indicated that materials of this type are less prone

to absorb electromagnetic radiation in comparison to nano-scale PAN fibres not containing nano-scale particles (Fig. 15).

For all PAN/nano-scale SiO_2 particle fibrous mats, absorption maxima were observed, falling to ultraviolet radiation band with wavelengths of 328 nm, wherein radiation absorption degree oscillated up to 0.76 for nano-scale composite fibres containing the smallest mass concentrations of nano-scale silica particles, amounting to 4%, through absorbance at the level of 0.83 for nano-scale PAN/8% SiO_2 fibres, up to ca. 1 for nano-scale fibres featuring maximum concentration of nano-scale silica particles (Fig. 15).

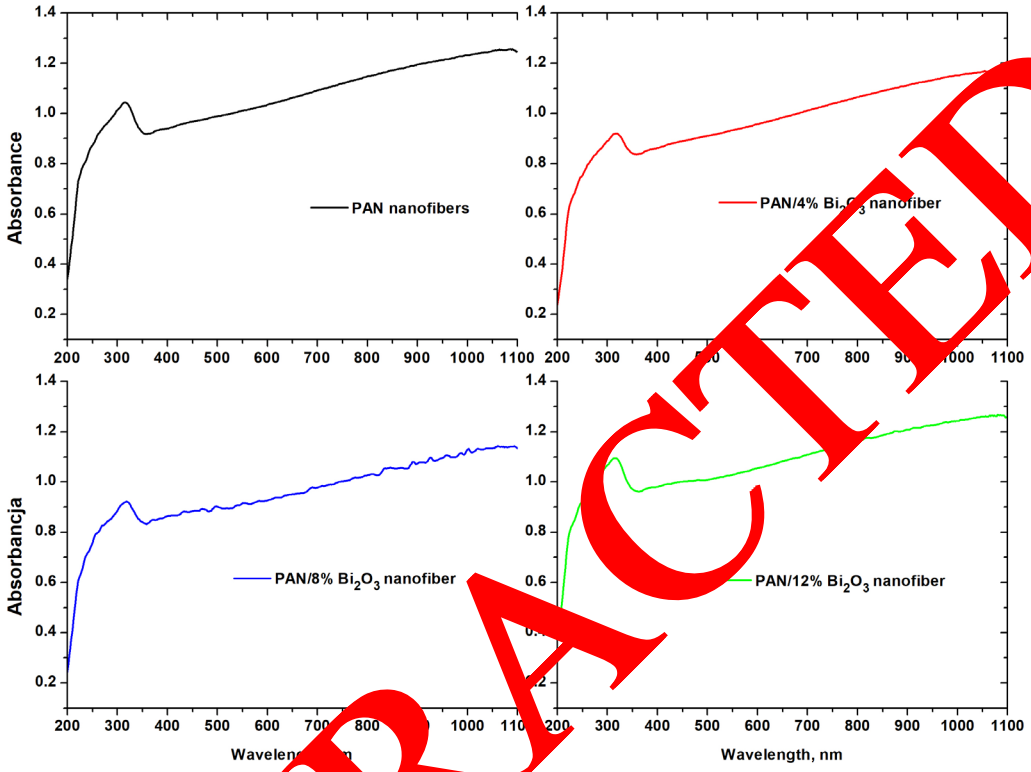

Fig. 14. UV-Vis absorbance spectra as a function of wavelength reaching the sample and obtained for nano-scale PAN fibres and nano-scale PAN/Bi_2O_3 composite fibres.

Also, in this case, there are bathochromic shifts of the sharp absorption edge of nano-scale composite fibres observed relative to fibres generated with 5% polyacrylonitrile solution in dimethylformamide, in spite of absorption edge falling below 230 nm, which is characteristic for pure nano-scale SiO_2 powder. This phenomenon is probably spurred by structural defects of nano-scale silica particles' surface, resultant of formation of incomplete Si-O-Si quadrilateral networks, which feature local optical activity — in this case, probably, corresponding to the so-called 'paramagnetic defects like E centres' [48].

Radiation absorption in the visible light and infrared band, observed for all types of generated nano-scale fibres (Fig. 13–15) is probably caused by, both, the nanometric diameters of fibres constituting the analysed fibrous mats, and the nanometric thickness of the very mats. The very high porosity of the analysed strata, stemming from their fibrous structure, additionally favours light absorption.

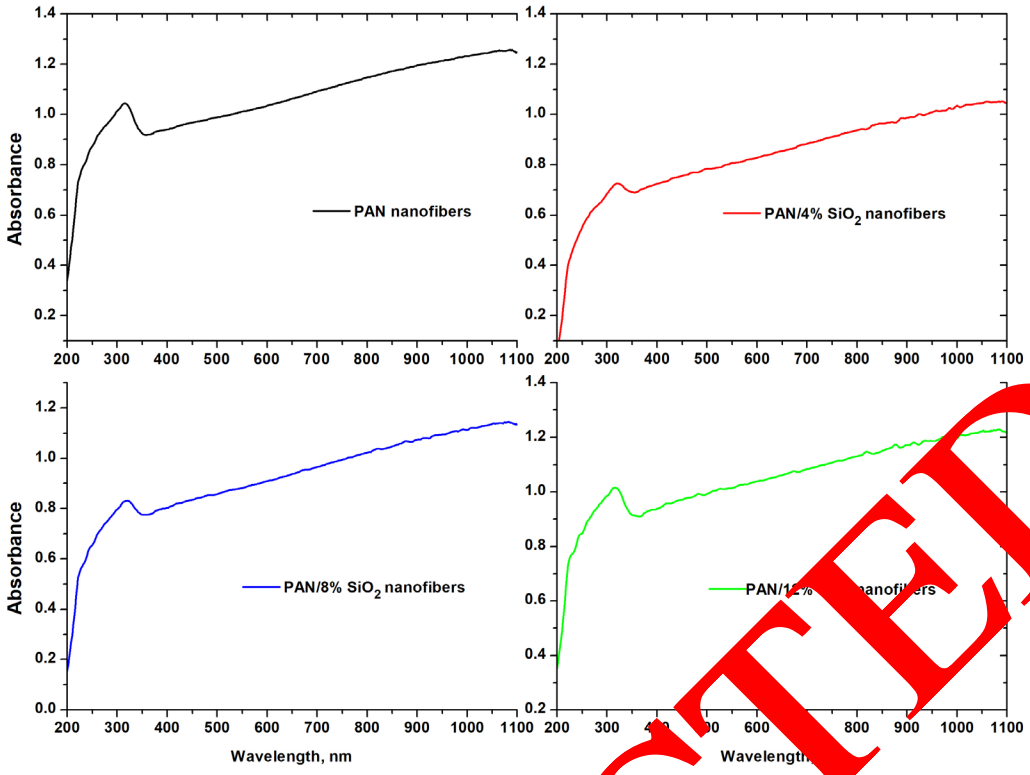

Fig. 15. UV-Vis absorbance spectra as a function of wavelength reaching the sample and obtained for nano-scale PAN fibres and nano-scale PAN/SiO_2 composite fibres.

On the basis of the determined resultant absorption spectra for the generated nano-scale polymer and composite fibres, and using a modified Swanepoel method, the following parameters were determined: value of the complex complex refractive index n, real part of refractive index n' as a function of the wavelength, extinction coefficient k as a function of the wavelength, complex dielectric constant, and real and imaginary part of the dielectric constant ε_r and ε_i as a function of the wavelength were all calculated. From the Beer–Lambert law and the relation between absorbance (A) and transmittance (T), the following was obtained:

$$A = log\frac{I_o}{I} = -log\,(T)\,, \tag{7}$$

where I_o is radiation intensity reaching an absorbing sample, and I is radiation intensity after passing through a sample.
Using the registered absorbance spectrum as a function of wavelength and the above equation, it is possible to determine transmittance as a function of wavelength:
Assuming the above relations and an equation:

$$T(\lambda) = 10^{-A(\lambda)}\,. \tag{8}$$

where h is the Planck constant, and ν is the frequency of radiation reaching a sample, it is possible to immediately introduce interdependencies with the coefficient of the analysed materials' absorption as a function of electromagnetic radiation wavelength:

$$\alpha(\lambda) = \ln\left(\frac{1}{10^{-A(\lambda)}}\right), \tag{10}$$

Using equation no. (10) and the relation between the absorption coefficient and the absorbance coefficient:

$$\alpha(\lambda) = \frac{4\pi k(\lambda)}{\lambda}\,, \tag{11}$$

A formulation for the extinction coefficient as a function of wavelengths is obtained:

$$k(\lambda) = \frac{1}{4\pi}\lambda \, ln\frac{1}{10^{-A(\lambda)}} \ . \tag{12}$$

When plotting the determined interdependence of transmittance (equation no. 8) as a function of radiation wavelength reaching the sample, it may be observed that the spectrum is characterised by interferences for higher values of transmittance.

The location of interference maxima and minima of the $T(\lambda)$ function is connected with the actual portion of the complex refraction coefficient of light:

$$n = n' + ik \ , \tag{13}$$

where n' is an actual portion of the refraction coefficient of light, and k is a extinction coefficient.

Further considerations were conducted with the use of Swanepoel method [49], which is restricted in applicability to thin solid strata on a transparent substrate, which is considerably thicker than the thickness of the analysed strata. The condition for the thickness of the obtained fibrous strata and for the substrate used is thus satisfied for samples generated and analysed within the scope of this paper. Based on the determined spectrum$10^{-A(\lambda)}$, the following step will be to determine limit values of transmittance $10^{-A(\lambda)}{}_{max}$ and $10^{-A(\lambda)}{}_{min}$ through execution of parabolic extrapolation of locations, in which subsequent function maxima and minima occur (Fig. 16). Following the determination of limit values $10^{-A(\lambda)}{}_{max}$ and $10^{-A(\lambda)}{}_{min}$, and using the interdependency

$$n = \left\{2n_p \frac{10^{-A(\lambda)}{}_{max} - 10^{-A(\lambda)}{}_{min}}{10^{-A(\lambda)}{}_{max}\ 10^{-A(\lambda)}{}_{min}} + \frac{{n_p}^2+1}{2} + \left[\left(2n_p \frac{10^{-A(\lambda)}{}_{max} - 10^{-A(\lambda)}{}_{min}}{10^{-A(\lambda)}{}_{max}\ 10^{-A(\lambda)}{}_{min}} + \frac{{n_p}^2+1}{2}\right)^2 - {n_p}^2\right]^{1/2}\right\}^{1/2} , \tag{14}$$

where n_p is the refraction coefficient of the used substrate; it is possible to determine the complex refraction coefficient of light for the analysed one-dimensional nano-scale polymer and composite structures.

Moreover, on the basis of the interdependency:

$$n = \varepsilon^{1/2} \ , \tag{15}$$

it is possible to determine at last the complex coefficient of dielectric constant, which is:

$$\varepsilon = 2n_p \frac{10^{-A(\lambda)}{}_{max} - 10^{-A(\lambda)}{}_{min}}{10^{-A(\lambda)}{}_{max}\ 10^{-A(\lambda)}{}_{min}} + \frac{{n_p}^2+1}{2} + \left[\left(2n_p \frac{10^{-A(\lambda)}{}_{max} - 10^{-A(\lambda)}{}_{min}}{10^{-A(\lambda)}{}_{max}\ 10^{-A(\lambda)}{}_{min}} + \frac{{n_p}^2+1}{2}\right) - {n_p}^2\right]^{1/2} , \tag{16}$$

Based on the derived interdependency of the extinction coefficient as a function of electromagnetic radiation wavelength reaching the sample $k(\lambda)$ and the determined reflection spectrum $R(\lambda)$, using the condition:

$$A(\lambda) + T(\lambda) + R(\lambda) = 1 \ , \tag{17}$$

it is possible to determine the actual portion of the refraction coefficient of light for the analysed nano-scale polymer and composite fibres. The real part of refractive index is then:

$$n'(\lambda) = \left\{\frac{4\,R(\lambda)}{[R(\lambda)-1]^2} - \left[\frac{1}{4\pi}\lambda \, ln\frac{1}{T(\lambda)}\right]^2\right\}^{1/2} - \frac{R(\lambda)+1}{R(\lambda)-1} \ . \tag{18}$$

Using relations between real $n'(\lambda)$ and imaginary $k(\lambda)$ part of the refractive index, the values of $\varepsilon_r(\lambda)$ and $\varepsilon_i(\lambda)$ are:

$$\varepsilon_r(\lambda) = n'(\lambda)^2 - k(\lambda)^2 , \tag{19}$$

$$\varepsilon_i(\lambda) = 2\, n'(\lambda)\, k(\lambda) . \tag{20}$$

In the final outcome, equations were derived, which describe interdependencies of the real $\varepsilon_r(\lambda)$ and imaginary $\varepsilon_i(\lambda)$ part of the complex permittivity:

$$\varepsilon_r(\lambda) = \left\{\left\{\frac{4\,R(\lambda)}{[R(\lambda)-1]^2} - \left[\frac{1}{4\pi}\lambda\, ln\frac{1}{T(\lambda)}\right]^2\right\}^{1/2} - \frac{R(\lambda)+1}{R(\lambda)-1}\right\}^2 - \left[\frac{1}{4\pi}\lambda\, ln\frac{1}{T(\lambda)}\right]^2 , \tag{21}$$

$$\varepsilon_i(\lambda) = 2\left\{\left\{\frac{4\,R(\lambda)}{[R(\lambda)-1]^2} - \left[\frac{1}{4\pi}\lambda\, ln\frac{1}{T(\lambda)}\right]^2\right\}^{1/2} - \frac{R(\lambda)+1}{R(\lambda)-1}\right\}\left[\frac{1}{4\pi}\lambda\, ln\frac{1}{T(\lambda)}\right] . \tag{22}$$

Based on the above transformations and resultant electromagnetic radiation absorbance spectra as a function of wavelength registered for the generated thin PAN fibrous mats and PAN/nano-scale TiO_2, Bi_2O_3 and SiO_2 composite particles, interdependencies were plotted for real $n'(\lambda)$ and imaginary $k(\lambda)$ part of the refractive index and real $\varepsilon_r(\lambda)$ and imaginary $\varepsilon_i(\lambda)$ part of the complex permittivity (Fig. 15–18). Moreover, complex values of n and ε were determined for all types of generated nano-scale fibres, which are presented in Tables 9 and 1

Table 9. Results of analyses of coefficients of refraction of light for the obtained fibrous strata generated with the distance between electrodes amounting to 20 cm, and with the use of the presented method.

Type of nanofibers		**Refractive index n**
PAN nanofibers		1.54
Composite nanofibers	PAN/ 4% TiO_2	1.67
	PAN/ 8% TiO_2	1.71
	PAN/12% TiO_2	1.75
	PAN/ 4% Bi_2O_3	1.68
	PAN/ 8% Bi_2O_3	1.74
	PAN/ 12% Bi_2O_3	1.78
	PAN/ 4% SiO_2	1.46
	PAN/ 8% SiO_2	1.55
	PAN/ 12% SiO_2	1.57

Table 10. Results of analyses of dielectric constant for the obtained fibrous strata generated with the distance between electrodes amounting to 20 cm, and with the use of the presented method.

Type of nanofibers		Dielectric constant ε
PAN nanofibers		2.38
Composite nanofibers	PAN/ 4% TiO_2	2.79
	PAN/ 8% TiO_2	2.91
	PAN/12% TiO_2	3.05
	PAN/ 4% Bi_2O_3	2.84
	PAN/ 8% Bi_2O_3	3.04
	PAN/ 12% Bi_2O_3	3.18
	PAN/ 4% SiO_2	2.03
	PAN/ 8% SiO_2	2.04
	PAN/ 12% SiO_2	2.48

Analyses conducted for the complex refraction coefficient of light for electrospun nano-scale PAN polymer fibres showed that those fibres featured the smallest determined value of the refraction coefficient of light amounting to 1.54, with the value provided by the manufacturer, Sigma Aldrich, amounted to 1.51. The similarity of values of the refraction coefficient of light provided by the manufacturer and determined experimentally with the described method may, already at this stage, prove its correctness and application potential. The slight discrepancy of the results, relative to the manufacturer's declared value stems probably from the morphology of the analysed fibrous polyacrylonitrile strata, for a thin fibrous mat was used for analysis, contrary to a solid stratum or an ampoule with polymer granulate. For the generated groups of nano-scale composite fibres reinforced with ceramic powders, an increase in optical densities was observed, accompanying an increase in the content of the mass concentration of the reinforcement phase, which matches the results of analyses conducted with the ellipsometric technique. Also, in this case, the smallest increase in coefficients of optical permeability determined for nano-scale PAN composite fibres reinforced with nano-scale SiO_2 particles is spurred by a relatively low value of optical permeability of the ceramic reinforcement employed, oscillating within the visible light band amounting to 1.45. The determined values n were in the range of 1.46 for fibres with 4% mass content of silica, through 1.55 for a concentration equalling 8%, up to 1.57 for nano-scale PAN fibres, containing the largest number of nano-scale SiO_2 particles.

Values of refraction coefficient of light for the generated PAN composites, reinforced with titanium and bismuth oxides were similar to each other, which matches the results obtained with the use of the spectroscopic ellipsometry technique. For nano-scale polyacrylonitrile fibres reinforced with titanium oxide particles, the values of coefficients of refraction of light amounted to, respectively, 1.67, 1.71 and 1.75, and their values increased concurrently with the presence of nano-scale ceramic powder in the polymer matrix. For nano-scale PAN fibres containing bismuth oxide, the same tendency was observed for an increase of the values of coefficients of refraction of light, accompanying a greater mass concentration of Bi_2O_3 in polyacrylonitrile. In this case, the values n increase from 1.68, through 1.74, and up to 1.78, respectively for PAN/4%, 8% and 12% Bi_2O_3 fibrous strata.

From the considerations discussed above, during a theoretical description of the presented method it is evidenced that together with an increase of the refraction coefficient of light for the analysed medium, its permittivity also increases. Determined on the basis of the presented considerations and

resultant spectra$A(\lambda)$, the complex values of the permittivity of the generated nano-scale PAN polymer fibres and nano-scale PAN/nano-scale TiO_2, Bi_2O_3 and SiO_2 particle composite fibres (Tab. 10) match the theoretical assumptions, stemming from an interdependency of $n = \varepsilon^{1/2}$. With an increase of concentrations of the used nano-scale ceramic particles in a polymer matrix, there was an increase in coefficients of refraction of light for the analysed media, and thus an increase of the determined values of permittivity.

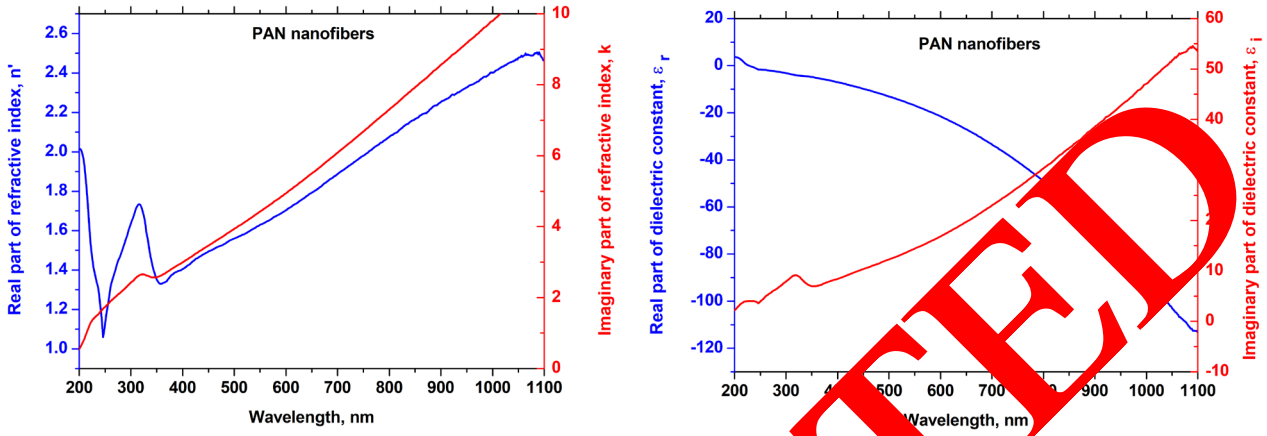

Fig. 16. Dependence of the real $n'(\lambda)$ and imaginary $k(\lambda)$ part of the refractive index, as well as real $\varepsilon_r(\lambda)$ and imaginary $\varepsilon_i(\lambda)$ part of the complex permittivity, determined for the generated nano-scale PAN polymer fibres.

Fig. 16 shows comparison of interdependencies of the real $n'(\lambda)$ and imaginary $k(\lambda)$ part of the refractive index determined through the usage of spectroscopic ellipsometry by Richard Galos' team [37] for a fibrous mat consisting in electrospun nano-scale PZT fibres and exemplary real $n'(\lambda)$ and imaginary $k(\lambda)$ part of the refractive index, determined with the use of a method presented in this paper for electrospun nano-scale PAN/SiO_2 composite fibres. As it may be seen, interdependencies $n'(\lambda)$ and $k(\lambda)$ part of the refractive index determined for nano-scale PZT fibres differ considerably with relation to characteristics obtained for the solid PZT strata, which were presented in Galos' paper [37]. This fact confirms unequivocally that despite the employment of the same material for the generation of both solid PZT stratum and thin fibrous stratum generated with electrospinning method; the obtained materials differ in terms of their own optical features. The observed differences in charts $n'(\lambda)$ and $k(\lambda)$ were triggered by the morphology of the analysed fibrous strata (space between fibres and surface coarseness of the analysed fabric) relative to solid PZT strata.

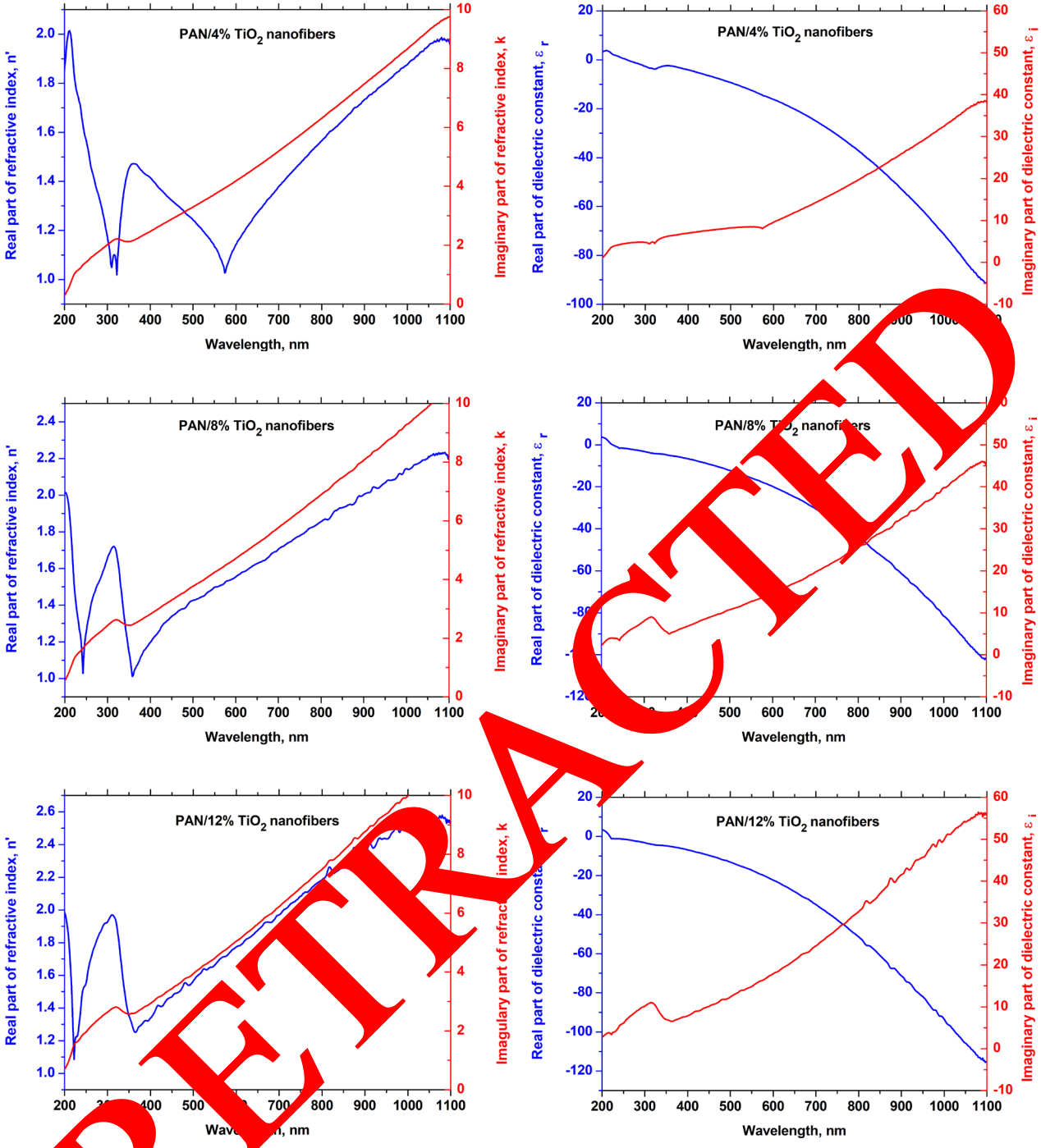

Fig. 1 Dependence of the real $n'(\lambda)$ and imaginary $k(\lambda)$ part of the refractive index, as well as real $\varepsilon_r(\lambda)$ and imaginary $\varepsilon_i(\lambda)$ part of the complex permittivity, determined for the generated nano-scale PAN/TiO_2 composite fibres.

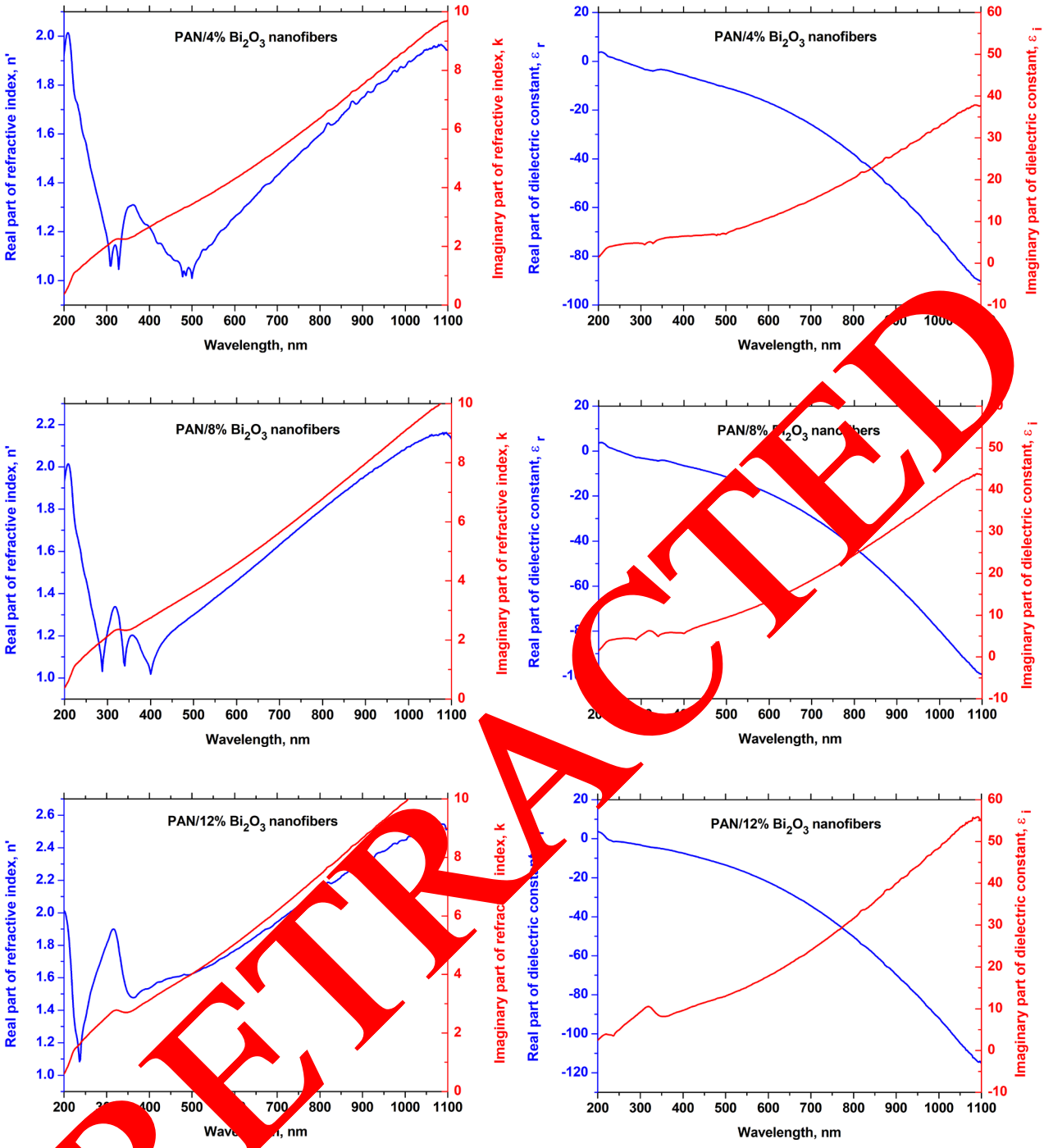

Fig. 18. Dependence of the real $n'(\lambda)$ and imaginary $k(\lambda)$ part of the refractive index, as well as real $\varepsilon_r(\lambda)$ and imaginary $\varepsilon_i(\lambda)$ part of the complex permittivity, determined for the generated nano-scale PAN/Bi_2O_3 composite fibres.

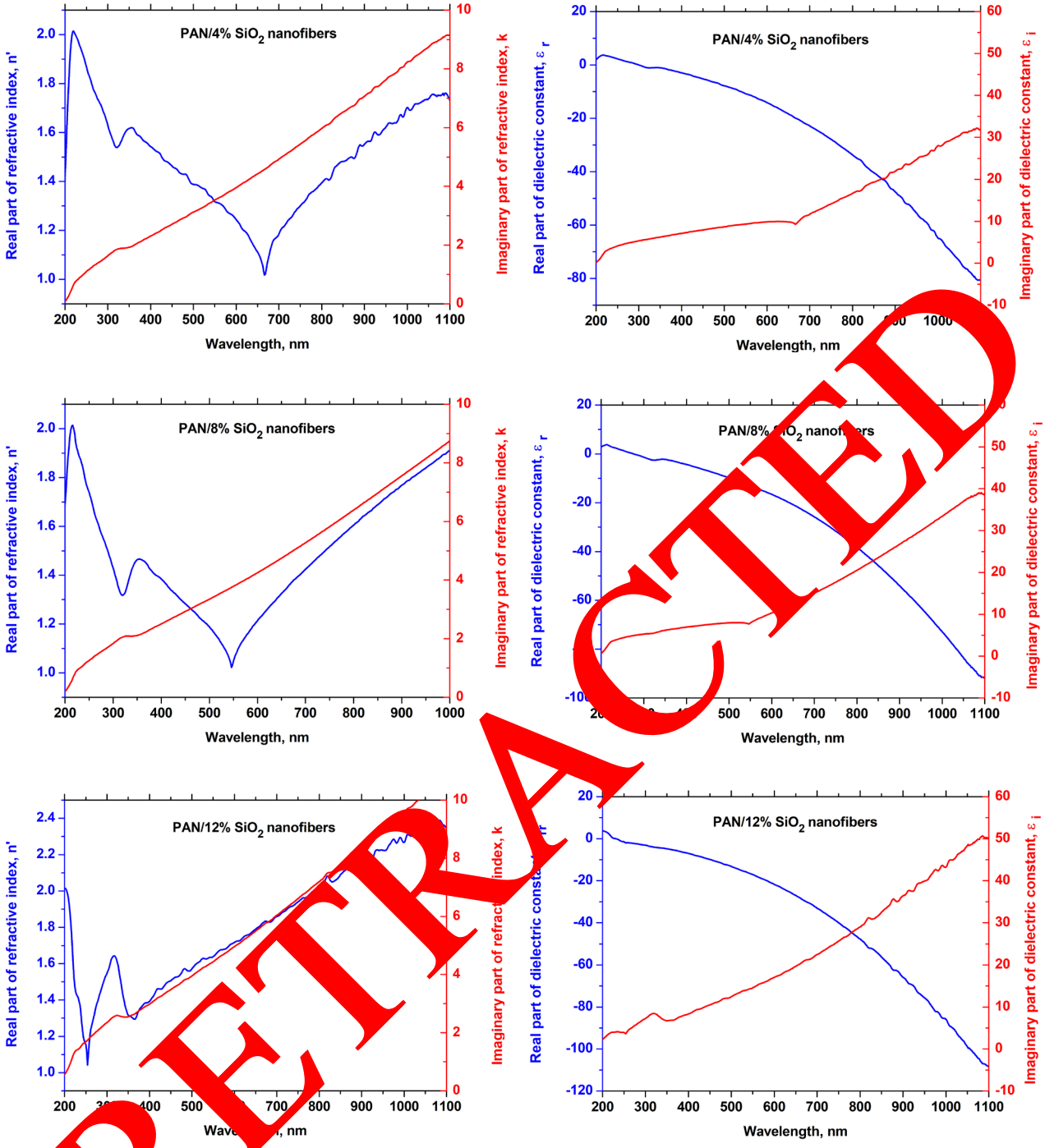

Fig. 19. Dependence of the real $n'(\lambda)$ and imaginary $k(\lambda)$ part of the refractive index, as well as real $\varepsilon_r(\lambda)$ and imaginary $\varepsilon_i(\lambda)$ part of the complex permittivity, determined for the generated nano-scale PAN/SiO_2 composite fibres

The comparison of interdependencies presented in Figure 16-19 makes it clear that characteristics of the real $n'(\lambda)$ and imaginary $k(\lambda)$ part of the refractive index, determined with the use of spectroscopic ellipsometry method by Richard Galos' team are similar to the results obtained with the use of the method presented in this paper; this, in combination with the factual similarity of optical characteristics of PZT and materials that are subject of analysis in this paper, may clearly prove the correctness of the presented method for determination of optical constants of nano-scale polymer and composite fibres, based only on absorbance spectra as a function of radiation wavelength, determined with the use of UV-Vis spectrometer.

Summary

On the basis of results of own research, covering optimisation of production process and analysis of morphology, structure and optical characteristics of nano-scale PAN polymer and PAN composite fibres/nano-scale TiO_2, Bi_2O_3, SiO_2 particles, the following conclusions were formulated:

1. The diameter and concentration of nano-scale ceramic particles in a spinning solution have a considerable influence on the morphology of nano-scale composite fibres generated with their use. The usage of spinning solutions, featuring an increasing mass concentration of the reinforcement phase, within the range of 4–12% relative to the polymer mass, favours an increase of the diameters of the generated one-dimensional nano-scale composite structures. Additionally, the employment of nano-scale ceramic particles with diameters not exceeding 50 nm results in the generation of numerous structural defects of nano-scale composite fibres in the form of beads and agglomerates of nano-scale particles.
2. It is possible to design optical characteristics of one-dimensional nano-scale structures in the form of nano-scale composite fibres in a polymer matrix, reinforced with nano-scale semiconducting or dielectric particles through a selection of the mass concentration of the used reinforcement phase relative to the polymer matrix. On the basis of optical research conducted with the use of ellipsometric and UV-Vis spectroscopy techniques, it is proved that an increase of the mass concentration of nano-scale ceramic particles in composite fibres causes an increase of values of optical constants, i.e. refraction index and permittivity of the generated nano-scale composite fibres type PAN/nano-scale TiO_2, Bi_2O_3, SiO_2 particles. Wherein the obtained values of optical constants and forbidden band are greater than the values characteristic for pure polymer and smaller than values characteristic for the used oxide.
3. It is possible to determine optical constants (i.e. complex refractive index n, the real $n'(\lambda)$ part of the refractive index as a function of wavelength, imaginary $k(\lambda)$ part of the refractive index as a function of wavelength, complex dielectric constant, real and imaginary part of dielectric constant $\varepsilon_r(\lambda)$ and $\varepsilon_i(\lambda)$ as a function of wavelength) of one-dimensional nano-scale polymer or composite structures based only on absorbance spectra as a function of electromagnetic radiation wavelength reaching a sample, which were obtained with the use of a UV-Vis spectrometer. On the basis of the obtained UV-Vis spectra and the author's method based on a modified Swanepoel method, which, as a standard, is used to determination of optical constants of solid strata, the optical constants of the generated nano-scale polymer and composite fibres were determined, and a comparison of the final results with the results obtained with the use of the classic ellipsometric method proves the correctness of the considerations. The presented method may potentially become an attractive tool for a rapid and easy determination of the optical constants of nano-scale polymer and composite fibres generated with the use of electrospinning from a solution.

References

[1] Fong, H., Chun, I., & Reneker, D. H. (1999). Beaded nanofibers formed during electrospinning. Polymer, 40(16), 4585-4592.
[2] Reneker, D. H., Yarin, A. L., Fong, H., & Koombhongse, S. (2000). Bending instability of electrically charged liquid jets of polymer solutions in electrospinning. Journal of Applied physics, 87(9), 4531-4547.
[3] Tripatanasuwan, S., Zhong, Z., & Reneker, D. H. (2007). Effect of evaporation and solidification of the charged jet in electrospinning of poly (ethylene oxide) aqueous solution. Polymer, 48(19), 5742-5746.
[4] Reneker, D. H., & Chun, I. (1996). Nanometre diameter fibres of polymer, produced by electrospinning. Nanotechnology, 7(3), 216.
[5] Doshi, J., & Reneker, D. H. (1995). Electrospinning process and applications of electrospun fibers. Journal of electrostatics, 35(2-3), 151-160.
[6] Fong, H., Chun, I., & Reneker, D. H. (1999). Beaded nanofibers formed during electrospinning. Polymer, 40(16), 4585-4592.

[7] Kim, J. S., & Reneker, D. H. (1999). Mechanical properties of composites using ultrafine electrospun fibers. Polymer composites, 20(1), 124-131.
[8] Kim, J. S., & Reneker, D. H. (1999). Polybenzimidazole nanofiber produced by electrospinning. Polymer Engineering & Science, 39(5), 849-854.
[9] Srinivasan, G., & Reneker, D. H. (1995). Structure and morphology of small diameter electrospun aramid fibers. Polymer international, 36(2), 195-201.
[10] Fang, X. D. H. R., & Reneker, D. H. (1997). DNA fibers by electrospinning. Journal of Macromolecular Science, Part B: Physics, 36(2), 169-173.
[11] Patil, R., Tsukruk, V. V., & Reneker, D. H. (1992). Molecular packing at surfaces of oriented polyimide fiber and film observed by atomic force microscopy. Polymer Bulletin, 29(5), 557-563.
[12] Yarin, A. L., Koombhongse, S., & Reneker, D. H. (2001). Bending instability in electrospinning of nanofibers. Journal of applied physics, 89(5), 3018-3026.
[13] Yarin, A. L., Koombhongse, S., & Reneker, D. H. (2001). Taylor cone and jetting from liquid droplets in electrospinning of nanofibers. Journal of applied physics, 90(9), 4836-48
Newsome, T. E., & Olesik, S. V. (2014). Electrospinning silica/polyvinylpyrrolidone composite nanofibers. Journal of Applied Polymer Science, 131(21).
[14] Prahsarn, C., Klinsukhon, W., & Roungpaisan, N. (2011). Electrospinning of PAN/DMF/H 2 O containing TiO 2 and photocatalytic activity of their webs. Materials Letters, 65(15), 2498-2501.
[15] Im, J. S., Kim, M. I., & Lee, Y. S. (2008). Preparation of PAN-based electrospun nanofiber webs containing TiO 2 for photocatalytic degradation. Materials Letters, 62(21), 3652-3655.
[16] Jeun, J. P., Park, D. W., Seo, D. K., Kim, H. B., Nho, Y. C., & Kang, P. H. (2011). Enhancement of photocatalytic activity of pan-based nanofibers containing sol-gel-derived TiO2 nanoparticles by E-beam irradiation. Reviews on Advanced Material Science, 28(1), 26-30
[17] Ji, B. C., Bae, S. S., Rabbani, M. M., & Yeum, J. H. (2013). Photocatalytic Activity of Electrospun PAN/TiO_2 Nanofibers in Dye Photodecomposition. 한국염색가공학회지, 25(2), 94-101.
[18] Ji, L., Saquing, C., Khan, S. A., & Zhang, X. (2008). Preparation and characterization of silica nanoparticulate–polyacrylonitrile composite and porous nanofibers. Nanotechnology, 19(8), 085605.
[19] Ji, L., & Zhang, X. (2008). Ultrafine polyacrylonitrile/silica composite fibers via electrospinning. Materials Letters, 62(14), 2161-2164.
[20] Ji, L., Lin, Z., Medford, A. J., & Zhang, X. (2009). Porous carbon nanofibers from electrospun polyacrylonitrile/SiO 2 composites as an energy storage material. Carbon, 47(14), 3346-3354.
[21] Wang, N., Si, Y., Wang, N., Sun, G., El-Newehy, M., Al-Deyab, S. S., & Ding, B. (2014). Multilevel structured polyacrylonitrile/silica nanofibrous membranes for high-performance air filtration. Separation and Purification Technology, 126, 44-51.
[22] Leontie, L., Caraman, M., Delibaş, M., & Rusu, G. I. (2001). Optical properties of bismuth trioxide thin films. Materials Research Bulletin, 36(9), 1629-1637.
[23] Zhang, L., Ishimoto, Y., Taishi, T., Nakamura, I., & Ni, Q. Q. (2011). Fabrication of flower-shaped Bi_2O_3 superstructure by a facile template-free process. Applied Surface Science, 257(15), 6577-6582.
[24] Nowakowski, D., Janiczek, T., Mielcarek, W., & Gajewski, J. B. (2009). Fractional electrical model for modified bismuth oxide. Journal of Electrostatics, 67(1), 18-21.
[25] Wang, Y., Zhao, J., & Wang, Z. (2011). A simple low-temperature fabrication of oblique prism-like bismuth oxide via a one-step aqueous process. Colloids and Surfaces A: Physicochemical and Engineering Aspects, 377(1), 409-413.
[26] An, T., Pant, B., Kim, S. Y., Park, M., Park, S. J., & Kim, H. Y. (2017). Mechanical and optical properties of electrospun nylon-6, 6 nanofiber reinforced cyclic butylene terephthalate composites. Journal of Industrial and Engineering Chemistry, 55, 35-39.
[27] Li, B., Pan, S., Yuan, H., & Zhang, Y. (2016). Optical and mechanical anisotropies of aligned electrospun nanofibers reinforced transparent PMMA nanocomposites. Composites Part A: Applied Science and Manufacturing, 90, 380-389.

[28] Barakat, N. A., Khil, M. S., Sheikh, F. A., & Kim, H. Y. (2008). Synthesis and optical properties of two cobalt oxides (CoO and Co3O4) nanofibers produced by electrospinning process. The Journal of Physical Chemistry C, 112(32), 12225-12233.
[29] Chuangchote, S., Sagawa, T., & Yoshikawa, S. (2008). Fabrication and optical properties of electrospun conductive polymer nanofibers from blended polymer solution. Japanese Journal of Applied Physics, 47(1S), 787.
[30] Weng, S., Lin, Z., Chen, L., & Zhou, J. (2010). Electrochemical synthesis and optical properties of helical polyaniline nanofibers. Electrochimica Acta, 55(8), 2727-2733.
[31] Wannapop, S., Thongtem, T., & Thongtem, S. (2012). Photoemission and energy gap of MgWO 4 particles connecting as nanofibers synthesized by electrospinning–calcination combinations. Applied Surface Science, 258(11), 4971-4976.
[32] Ren, Z., Jing, G., Liu, Y., Gao, J., Xiao, Z., Liu, Z., ... & Shen, G. (2013). Pre-pe skite nanofiber: a new direct-band gap semiconductor with green and near infrared p luminesc ce. RSC Advances, 3(16), 5453-5458.
[33] Wang, Y., Ramos, I., & Santiago-Avilés, J. J. (2007). Optical bandgap and photo nduc tance of electrospun tin oxide nanofibers. Journal of Applied Physics, 102(9), 0 3517.
[34] Wang, C., Shao, C., Wang, L., Zhang, L., Li, X., & Liu Y. 009). El ctrospinning preparation, characterization and photocatalytic properties of Bi 2 O 3 nanofi Jo nal of colloid and interface science, 333(1), 242-248.
[35] Viter, R., Katoch, A., & Kim, S. S. (2014). Grain siz depe nt bandgap shift of SnO2 nanofibers. Metals and Materials International, 20(1), 163
[36] Galos, R., Shi, Y., Ren, Z., Synowicki, R., Sun, H., Nykypanchuk, D., & Yuan, J. (2017). The dielectric constant of PZT nanofiber at visible and N R wavelengths. Nano-Structures & Nano-Objects.
[37] Dorywalski, K., & Patryn, A. (2014). Technika e rii spektroskopowej jako metoda monitorowania jakości powierzchni materiałów SrxBa1-xNb2O6. Przegląd Elektrotechniczny, 90(9), 22-25.
[38] Aspnes, D. E. (1982). Optical properties o hin films. Thin solid films, 89(3), 249-262.
[39] Fong, H.; Chun, I.; Reneker, D. H. Polymer 1999, 40, 4585–4592.
[40] Yanilmaz, M.; Lu, Y.; Zha Zh g, X. J. Power Sources 2016, 313, 205-212.
[41] Jalalah, M.; Faisal, M Bouzi ; Park, J.; Al-Sayari, S. A.; Ismail, A. A. J. Ind. Eng. Chem. 2015, 30, 183-189.
[42] Pankove J.I.(197) Op al Process s in Semiconductors. New York, NY, U.S.A.: Prentice Hall.
[43] Nirmala, R., Jeon, K., R amathavan, R., Kim, B. S., Khil, M. S., & Kim, H. Y. (2013). Fabrication and characterization II–VI semiconductor nanoparticles decorated electrospun polyacrylonitril anofi rs. Journal of colloid and interface science, 397, 65-72.
[44] Tański, T., tysiak, W., & Krzemiński, Ł. (2017). Analysis of optical properties of TiO2 nanopart nd PA TiO2 composite nanofibers. Materials and Manufacturing Processes, 32(11), 1218-1 24.
[45] uy H. O & Deng, B. (2012). Electrospinning and in situ nitrogen doping of TiO 2/PAN nanofibers ith photocatalytic activation in visible lights. Materials Letters, 82, 102-104
[46] Tańsk T., Matysiak, W., & Krzemiński, Ł. (2017). Analysis of optical properties of TiO2 nanoparticles and PAN/TiO2 composite nanofibers. Materials and Manufacturing Processes, 32(11), 1218-1224.
[47] Hezam, A., Namratha, K., Drmosh, Q. A., Yamani, Z. H., & Byrappa, K. (2017). Synthesis of heterostructured Bi 2 O 3–CeO 2–ZnO photocatalyst with enhanced sunlight photocatalytic activity. Ceramics International, 43(6), 5292-5301.
[48] Xu, X., Wang, M., Pei, Y., Ai, C., & Yuan, L. (2014). SiO 2@ Ag/AgCl: a low-cost and highly efficient plasmonic photocatalyst for degrading rhodamine B under visible light irradiation. RSC Advances, 4(110), 64747-64755
[49] Swanepoel, R. (1984). Determination of surface roughness and optical constants of inhomogeneous amorphous silicon films. Journal of Physics E: Scientific Instruments, 17(10), 896.